UC Berkeley
UC Berkeley Electronic Theses and Dissertations

Title
Biochemical and Biophysical Regulation of Cell Reprogramming

Permalink
https://escholarship.org/uc/item/81n7s6pv

Author
Soto, Jennifer

Publication Date
2016

Peer reviewed|Thesis/dissertation

Biochemical and Biophysical Regulation of Cell Reprogramming

by

Jennifer Soto

A dissertation submitted in partial satisfaction of the

requirements for the degree of

Joint Doctor of Philosophy
with University of California, San Francisco

in

Bioengineering

in the

Graduate Division

of the

University of California, Berkeley

Committee in charge:

Professor Song Li, Chair
Professor Tamara Alliston
Professor Liwei Lin

Fall 2016

Abstract

Biochemical and Biophysical Regulation of Cell Reprogramming

by

Jennifer Soto

Joint Doctor of Philosophy
with the University of California, San Francisco

in Bioengineering

University of California, Berkeley

Professor Song Li, Chair

Cell reprogramming, the reverse process of differentiation, represents a major advancement in cell biology and has wide applications in regenerative medicine, drug screening and disease modeling. Induced pluripotent stem cell (iPSC) reprogramming and direct conversion are two promising approaches to manipulate cell fate. Although extensive studies have been conducted on the role of chemical methods and biomaterials in iPSC reprogramming, their effect on direct reprogramming, the process of converting a somatic cell into a distantly related cell type while avoiding a pluripotent state, have not been fully explored. In this dissertation, we demonstrate, for the first time, that small molecules that disrupt the cytoskeleton, more specifically inhibitors of cell contractility, can significantly improve the direct reprogramming of adult fibroblasts into neurons by modulating gene and protein expression. Furthermore, our findings suggest that focal adhesions and the nuclear lamina play a critical role in this direct reprogramming process. In addition to soluble chemical factors from the microenvironment, the physical microenvironment can also strongly influence cellular processes. Thus, we investigated how biophysical factors regulated induced neuronal conversion. We explored the effects of topography on this process, utilizing poly(dimethylsiloxane) (PDMS) microgrooves and electrospun nanofibrous membranes as our bioengineered substrates in conjunction with lentiviral delivery of specific neurogenic transcription factors. We unraveled that nanoscale cues, in comparison to microscale cues, were more effective at promoting induced neuronal reprogramming. The derivation of induced neuronal cells using direct reprogramming not only serves to provide a platform for neurological disease modeling but moreover, holds great promise for personalized medicine as the generation of patient-specific cells can be valuable for drug discovery and the development of new therapeutics.

Dedication

This work is dedicated to my parents,
Oscar and Frida Soto,
and my brother, Jeff Soto,
whose love and support has given
me the strength to accomplish my goals.

Everything is possible when you have faith.

Acknowledgements

First and foremost, I would like to thank the God, for it is He who guides me through this journey. This dissertation would not have been possible without the help and support of many people. I would like to thank my family for all of their support and in particular my parents, for always encouraging me to pursue my dreams and supporting me along the way. To Venny, thank you for always supporting me and for joining me on this adventure. Although we are many miles apart, thank you Vanessa for being a great friend and for always being there for me.

I would also like to thank my PhD advisor, Dr. Song Li, for his mentorship and always encouraging me to dream big. To the previous and current Li lab members, thank you for all your input throughout the years and in particular, a special shout-out to the neuron reprogramming subgroup, it was great working alongside all of you. I also had an amazing opportunity to mentor some incredible undergraduate researchers, whose contributions aided in the progress of this dissertation. To Jason Zhang and Jovanny Guillen, thank you for all your hard work. Similarly, I would like to thank my collaborators, Drs. Shyam Patel, Cheen Euong Ang, Marius Wernig, Hyungju Park and Mu-ming Poo. Additionally, I would like to thank the members of my qualifying exam committee (Drs. David Schaffer, Tamara Alliston, Liwei Lin, and Dorian Liepmann) and dissertation committee (Drs. Song Li, Tamara Alliston, and Liwei Lin) for their guidance, encouragement and support throughout my PhD career. Moreover, I would like to thank my funding sources as they have financially supported me during my graduate school tenure and have enabled me to achieve my goals. These include the National Science Foundation Graduate Research Fellowship and the University of California, Berkeley Chancellor's Fellowship.

To cohort 2011, you are an amazing group of friends and it has been great going through this PhD venture with you all. I will truly miss our annual Fourth of July celebrations and Thanksgiving get-togethers as these were some of the highlights of my time in graduate school. To Paul, Dan, Matt, Pamela, Anusuya, Harrison, Freeman, Kunwoo, Elena, Annie, Martha and Shea, thank you for your friendship and all of the wonderful memories. Finally, thank you to LAGSES, the Latino/a Association of Graduate Students in Engineering and Science, for your support and for providing me with a sense of community. I am truly grateful for the incredible friendships and fun adventures that I got to experience through LAGSES, which will never be forgotten. To the past and present LAGSES board members, it was an amazing opportunity to work with you all to achieve great things and I hope we continue to stay strong in our mission!

Table of Contents

Chapter 1: Introduction

Chapter 2: Cytoskeletal Disruption Regulates Induced Neuronal Conversion

Chapter 3: Effect of Topography on Direct Reprogramming of Fibroblasts into Neurons

Chapter 4: Conclusion

References

List of Figures

Chapter 1

Chapter 2

Chapter 3

List of Tables

Chapter 2

Chapter 3

Chapter 1: Introduction

1.1 Dissertation Introduction

Stems cells have the ability to self-renew and differentiate. Depending on their potency, they can give rise to one or more cell types from various germ layers. During development, these cells become committed towards a particular lineage and proceed through a progenitor stage until reaching a mature state in a process known as differentiation. For a long time, it was believed that cell differentiation was a unidirectional process and the epigenetic state of differentiated cells could not be reverted back into a more primitive one. However, in the late 1950s, John Gurdon challenged these views when he demonstrated that the nucleus of a terminally differentiated *Xenopus* intestinal cell could give rise to a mature, fertile animal upon transplantation into an enucleated oocyte[1]. These early studies involving somatic cell nuclear transfer established the notion that the reverse process of differentiation is possible and it is now recognized as reprogramming.

Similarly, in 2006, Takahashi and Yamanaka discovered that induced pluripotent stem cells (iPSCs) can be generated from somatic cells via the forced expression of four transcription factors, *Oct4*, *Sox2*, *c-Myc* and *Klf4*[2]. The development of such an approach opened up the possibility that any cell type can be made from a somatic cell by first reprogramming them into an induced pluripotent stage and then directing their differentiation into a desired cell type under the appropriate culture conditions. Since then, direct reprogramming has emerged as a new method to manipulate cell fate. Direct reprogramming is the process of converting a somatic cell into a very distantly related cell type without proceeding through a pluripotent stage (Figure 1.1). Thus, it is able to bypass some of the issues that are associated with iPSCs and conventional direct differentiation protocols, which are time-consuming and challenging due to spontaneous differentiation. Moreover, this method offers the advantage of circumventing the teratoma potential that exists when using iPSCs. As a result, direct reprogramming provides a faster and more direct method of obtaining a desired cell type and it is a promising approach for personalized medicine as the derivation of patient-specific cells offers great potential for disease modeling and drug screening.

The first evidence of direct reprogramming was in the late 1980s when it was reported that the forced expression of MyoD, a transcription factor in the skeletal muscle lineage, could induce mouse embryonic fibroblasts to become stable myoblasts[3]. Since then many groups have shown that fibroblasts can be directly reprogrammed into other cell types, such neurons[4,5], cardiomyocytes[6], blood cell progenitors[7], and hepatocytes[8,9], using genetic manipulation. Along with transcription factors, many studies have also revealed that iPSC and direct reprogramming can be achieved using other methods, including proteins[10], episomal plasmids[11], mRNA[12], microRNAs[13,14], and small molecules[15–18]. More recently, biophysical factors have been identified as playing an influential role in cell reprogramming.

It is known that cells can sense and respond to the chemical and physical cues from the microenvironment to elicit changes in cell function and remodeling of the niche. A comprehensive understanding of this bidirectional interaction between cells and niches is crucial to guide our design of next-generation biomaterials in order to be able to accurately control cell fate in a precise and predictable manner. Biomaterials display properties that can be broadly categorized as biochemical or biophysical. Biochemical cues include soluble factors, ECM composition and immobilized ligands whereas the latter is comprised of topography, stiffness,

ligand patterning, shear stress, and cyclic stretching. It has been widely reported that biophysical factors can influence cellular processes, such as morphology[19,20], proliferation[21], migration[22-23], and differentiation potential of various adult stem cells[24–29]. However, how these biophysical cues regulate cell reprogramming is not well understood.

Therefore, in order to more accurately control cell fate, it is of the upmost importance to gain a better understanding of the underlying mechanisms by which various biophysical factors can influence cell reprogramming and further modulate signaling pathways, epigenetic and/or chromatin states. In an effort to provide insights into the mechanisms that determine cell fate, this dissertation explores how biochemical and biophysical inputs can regulate cell reprogramming (Figure 1.2). This work aims to broaden our understanding of cell-matrix interactions during lineage conversion and has important implications in the design and optimization of materials for broad biological applications.
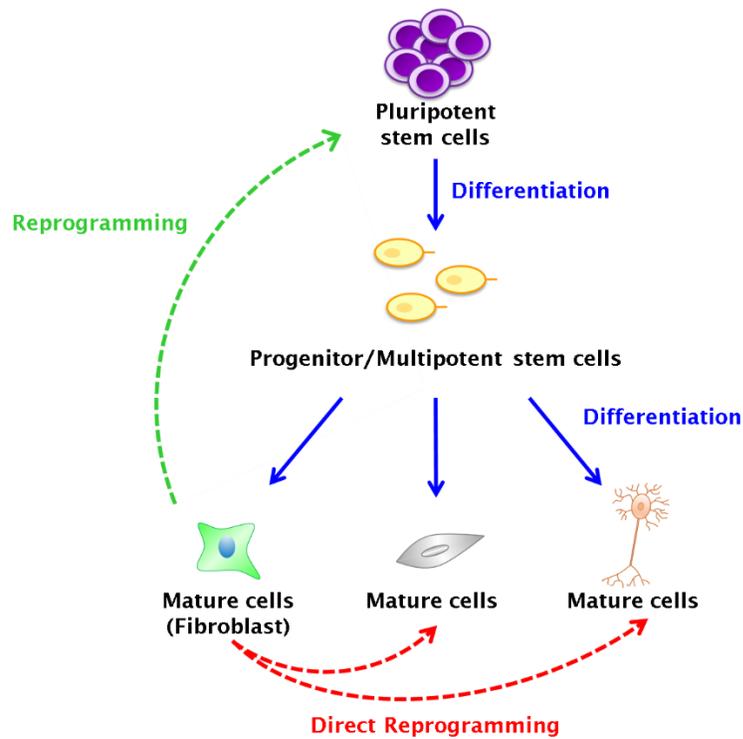
Figure 1.1 Cell reprogramming strategies. Schematic illustrating the process of differentiation, iPSC reprogramming, and direct conversion.

1.2 Dissertation Outline

In **Chapter 2**, we explore how the cytoskeleton may influence the direct reprogramming of fibroblasts into neurons using chemical compounds. We demonstrate that small molecules that disrupt the cytoskeleton enhance induced neuronal conversion. We show how these biochemical cues can alter gene and protein expression to regulate cell fate. Furthermore, we highlight the role of nuclear membrane proteins in this direct reprogramming process. Findings from this study will aid to advance our understanding of the role of the cytoskeleton and nucleoskeleton in direct conversion.

In **Chapter 3**, we demonstrate how biomaterials can regulate the direct conversion of fibroblasts into neurons. The effects of micro- and nanotopographical cues on the reprogramming efficiency are revealed. Additionally, we show that these biophysical factors did not hinder the derived cells from acquiring a mature neuronal phenotype. Altogether, this chapter highlights how topographical cues can be applied to further optimize cellular reprogramming.
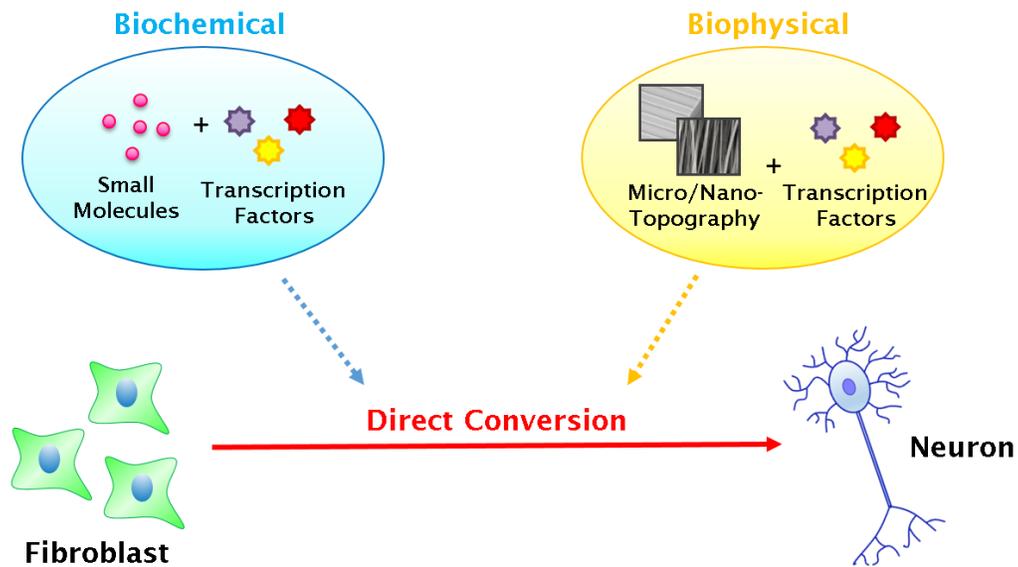
Figure 1.2 Overview of research goals. Schematic diagram highlighting the research goals of this dissertation which were to examine how biochemical and biophysical cues influence the direct reprogramming of fibroblasts into neurons.

Chapter 2: Cytoskeletal Disruption Regulates Induced Neuronal Conversion

2.1 Introduction

Cell reprogramming, the reverse process of differentiation, is an exciting approach for disease modeling and regenerative medicine. In contrast to induced pluripotent stem cell (iPSC) reprogramming, direct conversion offers a faster and more straightforward method of generating desired cell types from somatic cells. During this process, cells do not proceed through an intermediate pluripotent state, thus providing the ability to bypass some of the issues that exist with using iPSCs.

Previous works have demonstrated that with the use of genetic manipulation, fibroblasts can be directly converted into other cell types, including neurons[4,5], cardiomyocytes[6], blood cell progenitors[7], and hepatocytes[8,9]. In addition to transcription factors, it has been shown that microRNAs (miRNAs) can be used to induce lineage reprogramming of somatic cells[30–33]. Alongside these biochemical methods, it has also been revealed that biophysical factors play a critical role in regulating this process[34–36]. However, current direct reprogramming strategies are associated with low conversion efficiencies and the use of viral-based gene delivery limits the use of the derived cells for therapeutic purposes. Thus, recent efforts have focused on identifying small molecules that enhance the conversion efficiency and/or can be used to achieve direct conversion without the use of exogenous transcription factors. Interestingly, recent studies have shown that chemical cocktails can be used to directly convert fibroblasts into neurons and cardiomyocytes[16–18].

Although extensive studies have been performed on the role of transcription factors, miRNAs, biomaterials, and chemical compounds in direct reprogramming, little is known about how the cell cytoskeleton may influence this process. In eukaryotic cells, the cytoskeleton is a scaffold primarily composed of actin microfilaments, intermediate filaments and microtubules. The cytoskeleton spans the cytoplasm to provide a structural link between the cell nucleus and the extracellular matrix. Moreover, it serves to spatially organize contents of the cell and enables cells to be able to move and change shape through the generation of forces[37]. As the cytoskeleton is involved in many cellular processes, we hypothesized that it may play a pivotal role in cell fate conversion.

In order to elucidate the role of the cytoskeleton in direct reprogramming, we utilized the model of converting fibroblasts into neurons in conjunction with small molecule compounds that are known to modulate the cytoskeleton[4]. Here, we report that disruption of actin-myosin contractility via treatment with blebbistatin can enhance the efficiency of induced neuronal conversion. We demonstrate that blebbistatin can modulate the gene and protein expression of fibroblast and neuronal markers. In addition, blebbistatin can regulate focal adhesion kinase and disrupt the nuclear membrane protein, lamin A, to influence direct reprogramming. Moreover, we found that blebbistatin can be employed to improve the yield of iN cells derived with Ascl1 only. Overall, our findings highlight a novel role for the cytoskeleton in modulating the direct reprogramming process.

2.2 Materials and Methods

2.2.1 Fibroblast Isolation, Culture, and Reprogramming

Fibroblast isolation, culture, and reprogramming

Ear tissues from adult B57BL/6 mice were isolated, minced and partially digested in Liberase™ (0.025mg/ml, Roche) for 45 minutes under constant agitation at 37°C. Partially digested tissues were plated and fibroblasts were allowed to migrate out (passage 0). Isolated fibroblasts were expanded in MEF medium (DMEM+10% FBS [Corning] and 1% penicillin/streptomycin [GIBCO]) and used at passage 2 for all experiments. Fibroblasts from Tau-EGFP reporter mice (004779; The Jackson Laboratory) and lamin A/C mutant mice (009125; The Jackson Laboratory) were isolated as described above.

After transduction, mouse fibroblasts were seeded onto multi-well tissue culture-treated polystyrene dishes (Falcon) coated with laminin (0.1mg/ml, Corning). Twenty-four hours after seeding, the medium was replaced to MEF medium containing doxycycline (2µg/ml, Sigma). The following day the medium was changed to N3 medium (DMEM/F12 [GIBCO] + N2 supplement [Invitrogen] + B27 supplement [Invitrogen] + 1% penicillin/streptomycin [Gibco] + doxycycline [2µg/ml, Sigma]) and the cultures were maintained in this medium for the duration of the experiments. For Ascl1-only reprogramming, N3 medium was further supplemented with BDNF (5ng/ml, R&D systems) and GDNF (5ng/ml, R&D systems) after day 7. For cytoskeletal disruptions, Blebbistatin (Millipore), Y-27632 (Cayman Chemical), Nocodazole (Sigma), and PF573228 (Sigma) were used at the indicated concentrations. Culture medium was replenished every 2 days during reprogramming to maintain the activity of the small molecules. After culturing for the desired length (14 days for BAM and 21 days for Ascl1 only), the induced neuronal cells were analyzed and the reprogramming efficiency was determined.

Lentiviral production and cell transduction

Doxycycline-inducible lentiviral vectors for Tet-O-FUW-Ascl1, Tet-O-FUW-Brn2, Tet-O-FUW-Myt1l, and FUW-rtTA plasmids were used to transduce fibroblasts for ectopic expression of Ascl1, Brn2, Myt1l and rtTA. Lentivirus was made using established calcium phosphate transfection methods. Viral particles were collected and concentrated using Lenti-X Concentrator (Clontech) according to the manufacturer's protocol. Stable virus was aliquoted and stored at -80°C. For viral transduction, fibroblasts were seeded and allowed to attach overnight before incubation with virus and polybrene (8µg/ml, Sigma) for 24 hours. After incubation, transduced cells were reseeded onto laminin-coated tissue culture dishes.

2.2.2 Induced Neuronal Characterization and Quantification

Immunofluorescent staining and quantification

For immunostaining, cells were fixed with 4% paraformaldehyde, permeabilized with 0.5% Triton-X-100 (Sigma), and blocked with 5% donkey serum (Jackson Immunoresearch) in phosphate buffered saline (PBS). For actin-cytoskeleton staining, samples were incubated with

fluorescein isothiocyanate-conjugated phalloidin (Invitrogen) for 1 hour. Primary antibodies were incubated overnight at 4°C, followed by 1-hour incubation with Alexa 488 and/or Alexa 546 -labeled secondary antibodies (Molecular Probes). Nuclei were stained with 4,6-diamino-2-phenylindole (DAPI) (Invitrogen).

Two to three weeks after the addition of doxycycline, cultures were fixed and immunostained for neuronal beta-III tubulin (TUJ1). Induced neuronal cells were quantified using a Zeiss Axio Observer.D1 and identified based on displays of a typical neuronal morphology (defined as cells with a circular cell body containing a neurite that is at least three times the length of the cell body) and positive TUJ1 expression. The reprogramming efficiency was determined by quantifying the total number of TUJ1$^+$ iN cells in each condition and normalizing it to the number of cells plated at 24 hours post-seeding. Epifluorescence images were collected using a Zeiss Axio Observer.D1 and ImageXpress Micro XLS System (Molecular Devices) whereas confocal images were collected using a Zeiss LSM710 microscope. DAPI images were used to determine nuclear shape index and nuclear area. All image analyses were performed using ImageJ software.

2.2.3 Functional Assessment of Induced Neurons

Electrophysiology

All experiments were conducted at room temperature (22°C–24°C). All reagents were purchased from Sigma-Aldrich unless otherwise specified. Whole-cell recording was made from neurons using a patch clamp amplifier (MultiClamp 700B, Axon Instr.) under infrared differential interference contrast optics. Microelectrodes were made from borosilicate glass capillaries, with a resistance of 4–5 MW. For recording action potentials, cells were held at −70 mV in a voltage- clamp mode. The intracellular solution for whole-cell recording of EPSPs and action potentials contained (in mM) 140 potassium gluconate, 5 KCl, 10 HEPES, 0.2 EGTA, 2 MgCl$_2$, 4 MgATP, 0.3 Na$_2$GTP and 10 Na$_2$-phosphocreatine, pH 7.2 (adjusted with KOH).

For recording spontaneous EPSCs (sEPSCs), cells were pre-treated with the extracellular bath solution containing 50 μM picrotoxin (Tocris) to exclude an inhibitory synaptic activity and held at −70 mV in a voltage- clamp mode with the intracellular solution containing (in mM) 130 CsMeSO$_4$, 7 CsCl, 10 HEPES, 1 EGTA, 4 MgATP, 0.3 Na$_2$GTP, and 10 Na$_2$-phosphocreatine, pH 7.3 (adjusted with CsOH). After recording basal sEPSC responses for 5 min, 10 μM CNQX (Tocris) and 100 μM D,L-APV (Tocris) were co-treated to test whether sEPSCs were mediated by activation of both AMPA- and NMDA- type of glutamate receptors. For measuring spontaneous IPSC (sIPSCs), cells were pre-treated with the bath solution containing 10 μM CNQX and 100 μM D,L-APV and held at −70 mV with the intracellular solution containing (in mM) 137 CsCl, 10 HEPES, 1 EGTA, 4 MgATP, 0.3 Na$_2$GTP, and 10 Na$_2$-phosphocreatine, pH 7.3 (adjusted with CsOH). 50 μM picrotoxin was then treated to test a dependency of sIPSCs on GABA receptors after acquiring basal sIPSC responses for 5 min. Series resistance (10–25 MΩ) and input resistance (~200 MΩ using potassium-based internal solution; 1–2 GΩ using Cs-based internal solution) were monitored throughout the whole-cell recording or compared before and after sEPSC/IPSC recordings.

Off-line analyses of action potential properties (number, amplitude, half-width) and the

amplitude and frequency of sEPSC and sIPSC were performed by using a threshold event detection function of Clampfit software (Molecular Devices). Visualization of analysis results and their statistical tests were performed by using GraphPad Prism® 6.0 software.

2.2.4 Biochemical Analysis of Gene and Protein Expression

qRT-PCR

RNA was isolated from samples using Trizol® (Ambion) according to the manufacturer's instructions. For cDNA synthesis, 500 ng of RNA was reverse transcribed using Maxima First Strand cDNA Synthesis Kit (Thermo). Template DNA was amplified using Maxima SYBR Green/Fluorescein qPCR Master Mix (Thermo) on a CFX qPCR machine (Bio-Rad). qRT-PCR data were analyzed using CFX Manager 3.1 (Bio-Rad) and gene expression levels were normalized to 18S. Primers used for qRT-PCR are included in Table 2.1.

Western blots

Fibroblasts were lysed and collected in Laemmli buffer (0.0625mM Tris-HCl, 10% glycerol, 2% SDS,5% 2-mercaptoethanol, 0.002% bromophenol blue) containing RIPA buffer (50 mM Tris-HCl, 150 mM NaCl, 1% Triton-X-100, 0.1% SDS, 10 mM NaF, 0.5% sodium deoxycholate) along with protease inhibitors (PMSF, Na_3VO_4 and Leupeptin) on ice. Protein lysates were centrifuged to pellet cell debris, and the supernatant was collected and used in further analysis. Protein samples were run using SDS-PAGE and transferred to polyvinylidene fluoride (PVDF) membranes. Membranes were blocked in 3% nonfat milk and incubated with primary antibodies overnight. Primary antibodies include pFAK, FAK, αSMA, Calponin, Lamin A/C, Emerin, pERK, ERK, and GAPDH. Refer to Table 2.2 for all antibody information. Membranes were washed with Tris-Buffered Saline + 0.05% Tween-20 and incubated with HRP-conjugated IgG secondary antibodies (Santa Cruz Biotechnologies) for one hour. Protein bands were visualized using Western Lightning™ Plus - Enhanced Chemiluminscence Substrate (Perkin Elmer Life & Analytical Sciences) and imaged on a ChemiDoc XRS system (Bio-Rad).

RNA interference

RNA interference was performed using control (Cat. No. D-00180-10-20) and On-TARGETplus Emd (Cat. No. L-040132-01-0005) siRNAs from Dharmacon. Transfections were performed using 100nM final concentration of siRNA and Lipofectamine® 2000 (Invitrogen) according to manufacturer's instructions.

Statistical Analysis

The data are presented as mean, plus one standard deviation, where $n \geq 3$. Comparisons among values for groups greater than two were performed using a one-way analysis of variance (ANOVA) and differences between groups were predominantly determined using a Dunnett's post-hoc test and in some cases a Tukey's post-hoc test. For comparison between two groups, a two-tailed, unpaired t-test was used. For all cases, p-values less than 0.05 were considered statistically significant and GraphPad Prism® 6.0 software was used for all statistical analysis.

Table 2.1 Primers used for qRT-PCR analysis

Gene Name	Forward Primer	Reverse Primer
Ascl1	GAAGCAGGATGGCAGCAGAT	TTTTCTGCCTCCCCATTTGA
Brn2	AGGGCGCAAACGGAAAA	GGCTTAGGGCATTTGAGGAAA
Myt1l	CTACAAGATGGACGTGGACTCTGA	GGAACTCGAACCCCTTTGG
TUBB3	GCGCCTTTGGACACCTATTC	CACCACTCTGACCAAAGATAAAGTTGT
MAP2	GCTGTGTGCTCCAAGTTTCA	AGCTGAGGAACCTTAATTCTTGC
Syn1	CAGCTCAACAAATCCCAGTCT	TCTCAGCTTTCACCTCGTCC
NeuroD1	CACGCAGAAGGCAAGGTGTC	TTTGGTCATGTTTCCACTTCCTGT
CNN1	GAGAAACAAGAGCGGAGATTTGA	GCCCATCTGCAGTCCAATG
ACTA2	CATCTTTCATTGGGATGGAGTCA	GTCAATATCACACTTCATGATGCTGTT
Eln	GGATAAAACGAGGCGCTGAGA	GGAACCCCTCCAGGCTGC
Dcn	TACCCGGATTAAAAGGTCGTG	CCCAAGAGACTTGTGCCAGA
EMD	GGGGACCTCACTTGTAGATGC	AGGCGCTCCCTATCCTTG
18S	GCCGCTAGAGGTGAAATTCTTG	CATTCTTGGCAAATGCTTTCG

Table 2.2 Antibody information for immunofluorescent staining and Western blot analysis

Antibody	Vendor	Catalog #	Dilution	Application
Tuj1	Covance	MMS435P	1:1000	IF
Tuj1	Covance	MRB435P	1:1000	IF
NeuN	Covance	SIG39860	1:100	IF
MAP2	Sigma	M9942	1:200	IF
Synapsin	Abcam	ab64581	1:200	IF
VGlut1	Millipore	MAB5502	1:200	IF
GABA	Sigma	A2052	1:500	IF
TH	Millipore	AB152	1:250	IF
Paxillin	Abcam	ab32084	1:100	IF
pFAK	Abcam	ab81298	1:100	IF
Calponin	Abcam	ab46794	1:100 1:1500	IF WB
αSMA	Abcam	ab32575	1:200 1:2000	IF WB
Lamin A/C	Santa Cruz	sc-6125	1:50 1:1000	IF WB
Emerin	Sigma	HPA000609	1:100 1:1500	IF WB
pFAK	Cell Signaling	3283S	1:1000	WB
FAK	Cell Signaling	3285S	1:1000	WB
GAPDH	Santa Cruz	sc-32233	1:1500	WB
pERK	Cell Signaling	4370	1:1000	WB
ERK	Cell Signaling	4695	1:1000	WB

2.3 Results and Discussion

2.3.1 Disruption of Cytoskeletal Contractility Enhances Induced Neuronal Reprogramming

To elucidate the role of the cytoskeleton on induced neuronal conversion, primary fibroblasts isolated from adult mice were transduced with doxycycline-inducible lentiviral vectors encoding the three key reprogramming factors, *Brn2*, *Ascl1*, and *Myt1l* (BAM). Following transduction, cells were seeded onto tissue culture polystyrene dishes coated with laminin. As illustrated in Figure 2.1A, the cultures were maintained in neuronal medium for 14 days, followed by fixation and immunostaining for neuronal β-III tubulin (TUJ1) to determine the reprogramming efficiency. Small molecules that disrupt the cytoskeleton were added to the culture medium to evaluate their effects on the reprogramming process. Induced neuronal (iN) cells were identified based on displays of a typical neuronal morphology (defined as cells with a circular soma extending processes that are at least three times the length of the cell body) and positive TUJ1 expression. First, we tested the effects of blebbistatin, a non-muscle myosin II inhibitor, on the direct reprogramming of fibroblasts into neurons. We observed that induced neuronal cells could be derived in the absence and presence of blebbistatin (Figure 2.1B). Interestingly, when fibroblasts were induced to reprogram in the presence of varying concentrations of blebbistatin, we observed a linear dose response such that the reprogramming efficiency improved as the concentration of the inhibitor increased (Figure 2.1C). We observed that 10 µM blebbistatin was able to increase the reprogramming efficiency by approximately a 4.5-fold compared to the control. As 10 µM blebbistatin was able to yield the highest number of iN cells, this concentration was used in all further experiments. This enhancement of the reprogramming efficiency by blebbistatin was also confirmed using mouse fibroblasts isolated from Tau-EGFP mice, whereby cells expressing the neuronal marker, Tau, are concomitantly labeled with GFP (Figure 2.2A-B).

Blebbistatin is known to disrupt the cytoskeleton by inhibiting myosin II adenosine triphosphatase (ATPase) activity, resulting in a cell's inability to generate tension[38–40]. To distinguish whether the blebbistatin-induced enhancement in the reprogramming efficiency was due to an inhibition of cell contractility or simply the disruption of cytoskeletal structures, we employed the use of two additional chemical inhibitors, Y-27632 and Nocodazole. Y-27632 functions by inhibiting the activity of Rho-associated coiled-coil forming protein serine/threonine kinase (ROCK) and can further prevent stress fiber formation and cell contraction[41]. On the other hand, Nocodazole affects the cytoskeleton by interfering with the dynamics of microtubules[42], one of the major components of the cytoskeleton. Interestingly, we observed a similar trend in the reprogramming efficiency of fibroblasts transduced with BAM and cultured in the absence and presence of various concentrations of Y-27632 (Figure 2.1D). Y-27632 was able to increase the yield of iN cells similar to blebbistatin, although to a lesser degree. Conversely, administering differing concentrations of Nocodazole during the reprogramming process resulted in a reduction in the reprogramming efficiency (Figure 2.1E). As microtubules play a critical role during neuronal development and can regulate several cellular functions, such as cell division, more detailed studies focusing on the concentration of Nocodazole used need to be performed[43]. Moreover, it has been reported that microtubule-disrupting agents can stimulate cell contractility[44], thus it should be further explored whether Nocodazole augments cytoskeletal tension in our system.

To further optimize the use of blebbistatin to manipulate cell fate, we then investigated the kinetics of blebbistatin during the reprogramming process. First, we determined how long the inhibitor should be administered by reprogramming transduced fibroblasts in the absence and presence of blebbistatin for various periods of time. Surprisingly, we found that administering blebbistatin for only 3 days was sufficient to enhance the reprogramming efficiency, suggesting that blebbistatin may function to influence the early phase of the reprogramming (Figure 2.3A). Culturing the cells with blebbistatin for longer resulted in slight increases in the conversion efficiency. However, to reduce cytotoxicity and minimize the exposure of the cells to the inhibitor while promoting direct conversion, we decided to only administer blebbistatin during the initial 7 days of reprogramming. Additionally, time course studies of the reprogramming process revealed that as early as day 5, blebbistatin was more efficient at generating iN cells and this trend was evident throughout the reprogramming procedure (Figure 2.3B). Moreover, blebbistatin was also able to improve the neuronal purity, which reflects the percentage of TUJ1$^+$ cells that are present at the end of the reprogramming experiment (Figure 2.3C). Altogether, this data suggests that disruption of actin-myosin contractility can enhance induced neuronal conversion.
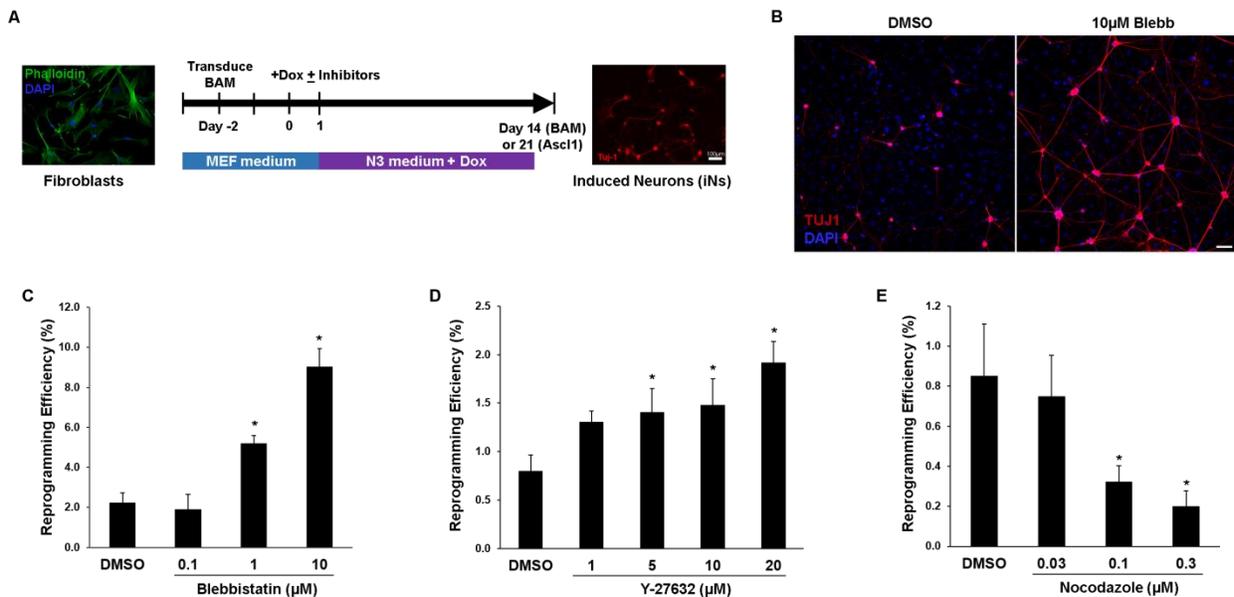
Figure 2.1 Inhibition of actomyosin contractility enhanced iN reprogramming efficiency. A. Reprogramming protocol. Adult fibroblasts transduced with the reprogramming factors were cultured in N3 medium for 14 days (BAM) or 21 days (Ascl1 only) before immunostaining and quantification. **B.** Representative fluorescent micrographs of iN cells generated from BAM-infected fibroblasts in the absence and presence of 10μM blebbistatin. iN cells expressed TUJ1 and formed neural networks (scale bar, 100μM). **C.** Reprogramming efficiency of fibroblasts transduced with BAM and cultured in absence and presence of varying concentrations of blebbistatin for 7 days, where DMSO served as a control. The number of biological replicates, n, was equal to 3 for this experiment. In all the figures, statistical significant differences are denoted as *, where $p < 0.05$ compared to the control. **D.** Reprogramming efficiency of BAM-transduced fibroblasts treated with increasing concentrations of the ROCK inhibitor, Y-27632, for 7 days (n=3). **E.** Reprogramming efficiency of fibroblasts transduced with BAM and treated with various concentrations of Nocodazole for 4 days (n=3).
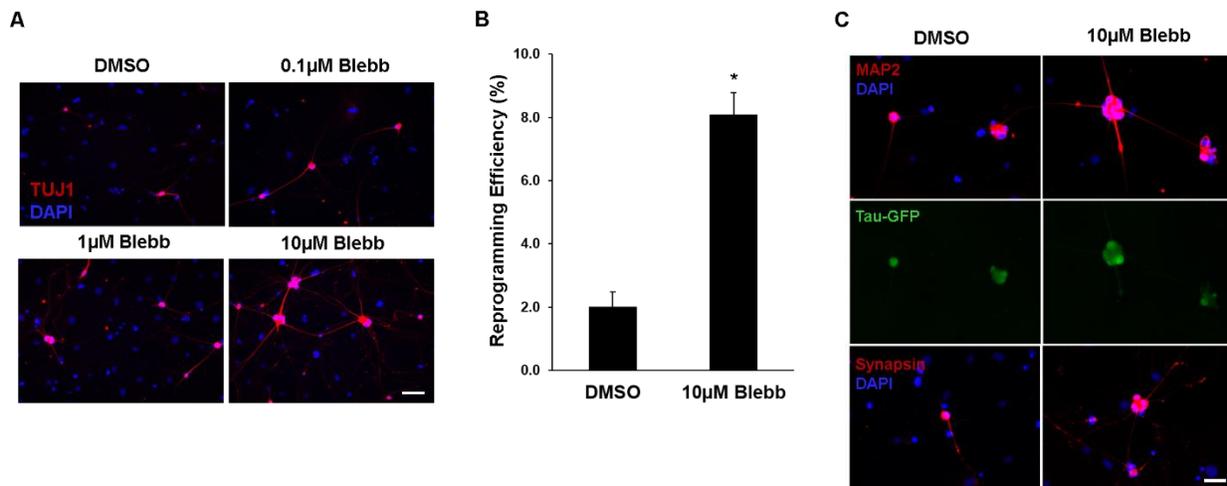
Figure 2.2 Blebbistatin can increase the conversion efficiency of Tau-EGFP fibroblasts. A. Immunofluorescent images show that iN cells derived from Tau-EGFP fibroblasts express TUJ1. **B.** Reprogramming efficiency of Tau-EGFP fibroblasts transduced with BAM and cultured in the presence of 10μM blebbistatin (n=4) (*p<0.05). **C.** Tau-EGFP fibroblast-derived iN cells co-express neuronal markers Tau-GFP, MAP2 and synapsin (scale bar, 50μm).
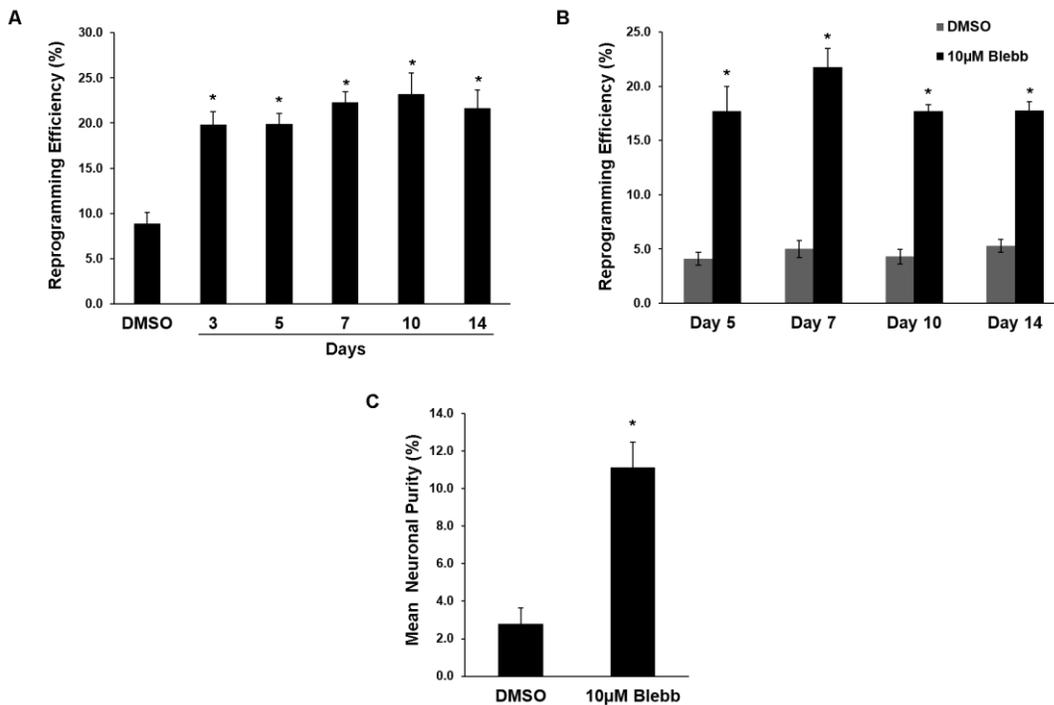
Figure 2.3 Blebbistatin can efficiently convert fibroblasts into neurons. A. Reprogramming efficiency after induction with BAM and treatment with 10μM blebbistatin for the indicated number of days (n=4). **B.** Reprogramming efficiency at various time points during the BAM reprogramming process. Blebbistatin (10μM) was administered for 7 days (n=3). **C.** Neuronal purity of cultures derived from BAM-reprogrammed fibroblasts treated with 10μM blebbistatin (n=7) (*p<0.05).

2.3.2 iN Cells Display Functional Neuronal Properties

Given we observed how the addition of blebbistatin could influence iN conversion efficiency, we then assessed the maturation and functionality of the derived iN cells. Immunostaining analysis for mature neuronal markers revealed that the iN cells expressed NeuN, microtubule-associated protein 2 (MAP2), and synapsin (Figure 2.4A). Similar observations were found in Tau-EGFP-derived iN cells (Figure 2.2C). Electrophysiological analysis indicated that the induced neurons were functional, exhibiting spontaneous changes in membrane potential in response to current injection (Figure 2.4B). Further analysis of several action potential properties showed no apparent difference for iN cells generated in the absence and presence of blebbistatin (Figure 2.5A-D). Although there was no significant difference in the frequency of spontaneous excitatory postsynaptic currents (EPSCs), the EPSC amplitude was significantly higher in iN cells derived with blebbistatin (Figure 2.5 F-G). Similarly, no significant difference in spontaneous inhibitory post synaptic currents (IPSCs) frequency was observed, however, the amplitude of IPSC was significantly lower in blebbistatin-derived iN cells (Figure 2.5I-J). Representative traces of spontaneous EPSCs and IPSCs can be found in Figure 2.5(E and H). Furthermore, iN cells were found to be of the GABAergic and glutamatergic subtypes, in agreement with previous reports that have used this combination of transcription factors[4] (Figure 2.6). Thus, the results suggest that the derived iN cells are mature and functional.
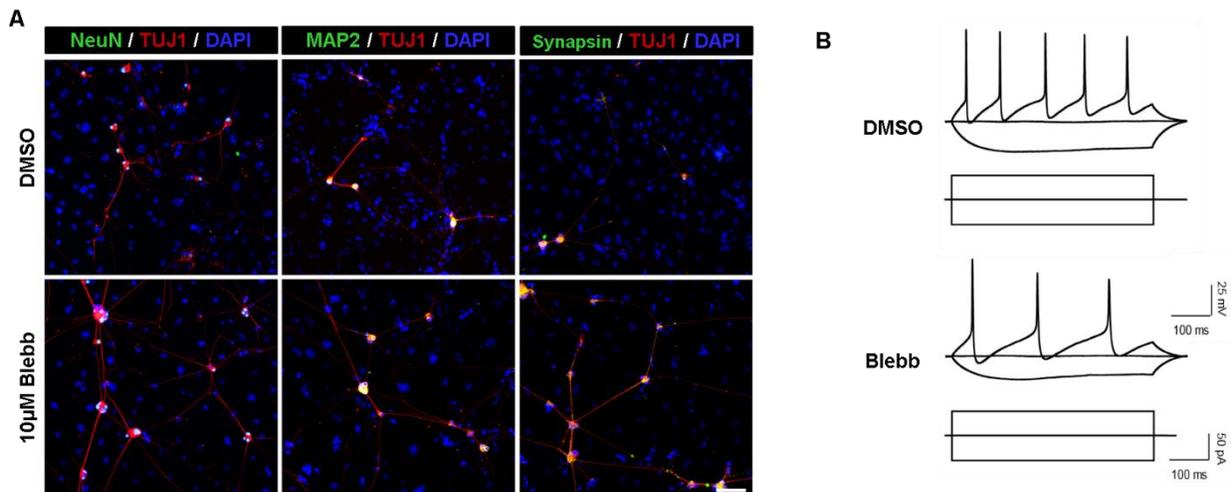
Figure 2.4 Induced neuronal cells exhibit functional neuronal properties. A. Representative fluorescent images of TUJ1^{+} iN cells co-expressing mature neuronal markers, NeuN, MAP2 and synapsin (scale bar, 100μm). **B.** Representative traces of spontaneous changes in membrane potential in response to current injection from iN cells obtained in the presence and absence of 10μM blebbistatin.
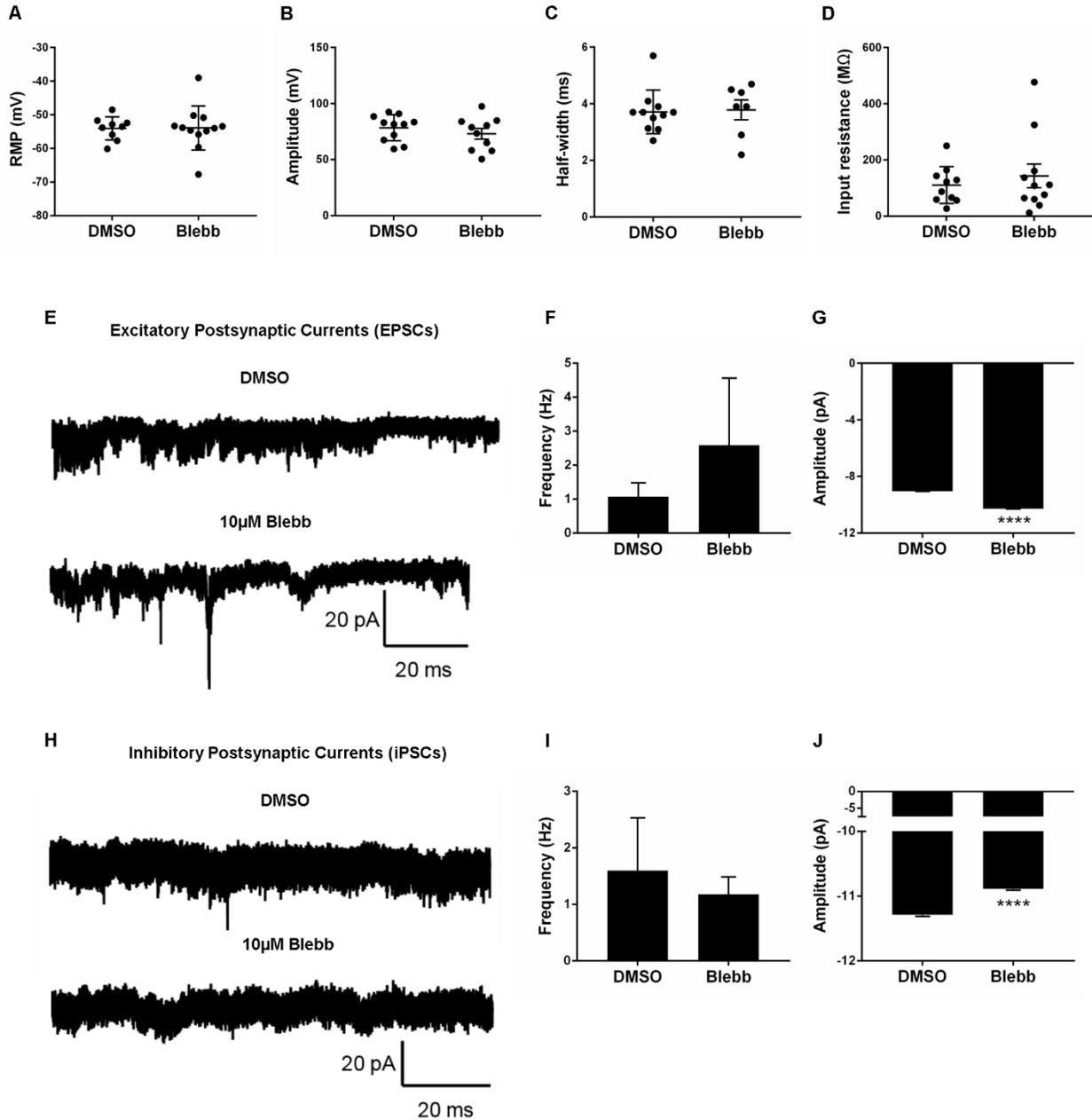
Figure 2.5 Functional assessment of derived iN cells by electrophysiological analysis. A-D. Quantification of electrophysiological properties of iN cells derived with and without blebbistatin. Each circle represents an individual cell that was tested. The resting membrane potential, RMP (A), action potential amplitude (B) and half-width (C) as well as input resistance (D) were measured. **E.** Representative recordings of spontaneous excitatory postsynaptic currents (EPSCs) from iN cells derived in the absence and presence of blebbistatin. **F-G.** Quantification of EPSC frequency and amplitude of iN cells (n=6). **H.** Representative traces of spontaneous inhibitory postsynaptic currents (IPSCs) in induced neurons derived in the absence and presence of blebbistatin. **I-J.** Quantification of IPSC frequency and amplitude of iN cells (n=4). Bar graphs represent mean $\pm$ one standard error of mean (****p<0.0001).
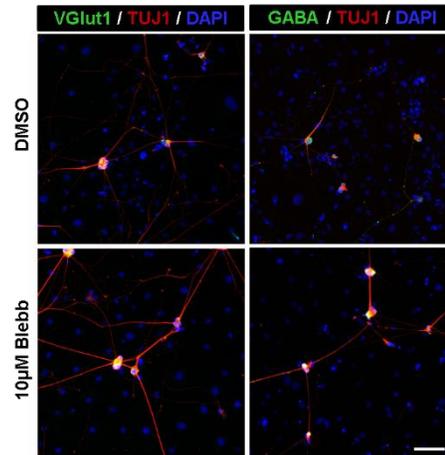
Figure 2.6 iN cells were identified as glutamatergic and GABAergic neuronal subtypes. Immunostaining images of TUJ1$^+$ iN cells expressing VGlut1 and GABA (scale bar, 100µm).

2.3.3 Blebbistatin Modulates Fibroblast and Neuronal Marker Expression

To gain insights into the mechanism by which blebbistatin can enhance the reprogramming efficiency, we first examined the effects of blebbistatin on cell morphology. We observed that blebbistatin induced dramatic changes in cell morphology and reduced cell spreading in fibroblasts treated with blebbistatin for 24 hours (Figure 2.7A). In addition, there appeared to be less intact actin fibers in fibroblasts treated with blebbistatin. Upon observing that cell spreading was affected, immunostaining analysis of focal adhesion proteins showed that blebbistatin led to a reduction in the number of positive paxillin punctate, suggesting that the inhibitor can modulate focal adhesions (Figure 2.7A). Furthermore, we found that although blebbistatin had no significant effect on the nuclear shape index, there were more cells that had a smaller nuclear area after a 2-hour treatment with the inhibitor (Figure 2.7B-C).

It has been proposed that reprogramming is a two phase process that involves the suppression of the original cell phenotype and the activation of the target cell fate regulatory program[16]. Thus, we investigated whether blebbistatin's mechanism of action involved the repression of the fibroblast program, in particular the loss of the mesenchymal phenotype. To test this, non-transduced fibroblasts were cultured with and without blebbistatin for 48 hours followed by analysis of mesenchymal marker expression. Interestingly, after blebbistatin treatment we observed less calponin and α-smooth muscle actin (SMA)-positive cells and the expression level for both genes had decreased (Figure 2.7D and 2.8A). Similarly, this trend was evident in fibroblasts transduced with BAM (Figure 2.7E and 2.8B). qRT-PCR analysis also showed the blebbistatin was able to downregulate the expression of fibroblast-associated genes, *Eln* and *DCN*, in non- and BAM-transduced fibroblasts (Figure 2.8C).

Consequently, we then explored the effect of blebbistatin on the second phase of reprogramming, the induction of the target cell phenotype. Non-transduced and BAM-transduced fibroblasts were cultured in the absence and presence of blebbistatin for 4 days at which point samples were collected and qRT-PCR analysis was performed to evaluate neuronal gene expression. We found that the expression of various neuronal genes, including the key reprogramming factors, were higher in cells transduced with BAM and treated with blebbistatin (Figure 2.7F). A similar trend was observed in samples that were collected after 14 days in culture (Figure 2.9C). To determine if blebbistatin could influence the expression of the reprogramming factors, we analyzed the expression of BAM at earlier time points. A time course

study on the expression of Ascl1 in non-transduced and BAM-transduced fibroblasts cultured with and without blebbistatin revealed that blebbistatin can upregulate Ascl1 expression in transduced fibroblasts and this can be seen as early as day 2, which is 24 hours after the addition of the inhibitor (Figure 2.9A). However, Brn2 and Myt1l did not show such as drastic increase in the expression level, suggesting that blebbistatin may enhance iN conversion efficiency by modulating Ascl1 expression (Figure 2.9B). It remains to be further examined whether blebbistatin can directly promote neuronal gene expression. In short, blebbistatin may influence iN conversion by inducing cell morphological changes and altering gene expression.

2.3.4 Inhibition of Focal Adhesion Kinase Improves iN Cell Generation

Focal adhesions (FAs) are large, multiprotein complexes that provide a physical link between the extracellular matrix and the cytoskeletal contractility machinery. Mechanotransduction refers to the process through which cells can sense and respond to mechanical signals by converting them into biochemical signals. FAs not only serve as mechanosensors since they can be modulated by biochemical and biophysical cues found in the microenvironment but moreover, can function as mechanotransducers to activate signaling pathways that regulate cytoskeletal organization[45]. Given we had observed that focal adhesions were affected by blebbistatin, we further examined whether focal adhesion signaling played a role in the direct reprogramming of fibroblasts into neurons. Western blot analysis revealed that blebbistatin negatively regulates focal adhesion kinase (FAK) phosphorylation at Tyrosine 397, a site crucial to initiate focal adhesion signaling, in BAM-transduced fibroblasts. We observed that FAK phosphorylation decreased as the blebbistatin concentration increased (Figure 2.10A). This was further confirmed in non-transduced fibroblasts using immunocytochemistry (Figure 2.10B).

To determine whether FAK inhibition can influence induced neuronal conversion, we first obtained and verified the specificity and potency of the focal adhesion kinase inhibitor, PF573228. Indeed, we found by Western blot analysis that PF573228 can inhibit the phosphorylation of FAK at Tyr-397 in a dose dependent manner (Figure 2.11A). In addition, we found that the inhibitor can modulate downstream ERK signaling. Immunostaining analysis also confirmed that PF573228 can reduce pFAK staining in fibroblasts (Figure 2.11B). Fibroblasts transduced with BAM were then induced to reprogram in the absence and presence of varying concentrations of PF573228. We found that PF573228 can increase the reprogramming efficiency in a dose dependent manner, similar to our findings with blebbistatin and Y-27632 (Figure 2.10C). As PF573228 can also influence ERK signaling, we found that the conversion efficiency was not significantly altered when BAM-transduced fibroblasts were treated with various doses of the ERK inhibitor, U0126, suggesting that the inhibition of FAK signaling, rather than ERK, plays a pivotal role in regulating iN conversion efficiency (Figure 2.11C). Further characterization of the iN cells derived in absence and presence of the FAK inhibitor showed that these cells expressed neuronal markers, including NeuN, MAP2, and synapsin (Figure 2.10D) and exhibited functional neuronal properties as assessed by electrophysiological analysis (Figure 2.12).

Subsequently, we examined whether FAK inhibition can modulate mesenchymal and neuronal marker expression similar to blebbistatin. Indeed, we found that calponin and αSMA expression were decreased in BAM-transduced fibroblasts that were treated with PF573228 for 2 days (Figure 2.10E). Conversely, neuronal gene expression was greater in fibroblasts transduced with BAM and cultured in the presence of 5μM PF573228 for 4 days (Figure 2.10F). Contrary to

blebbistatin, Ascl1 expression was not upregulated with the FAK inhibitor. Altogether, these findings demonstrate that focal adhesion kinase inhibition can regulate iN conversion.
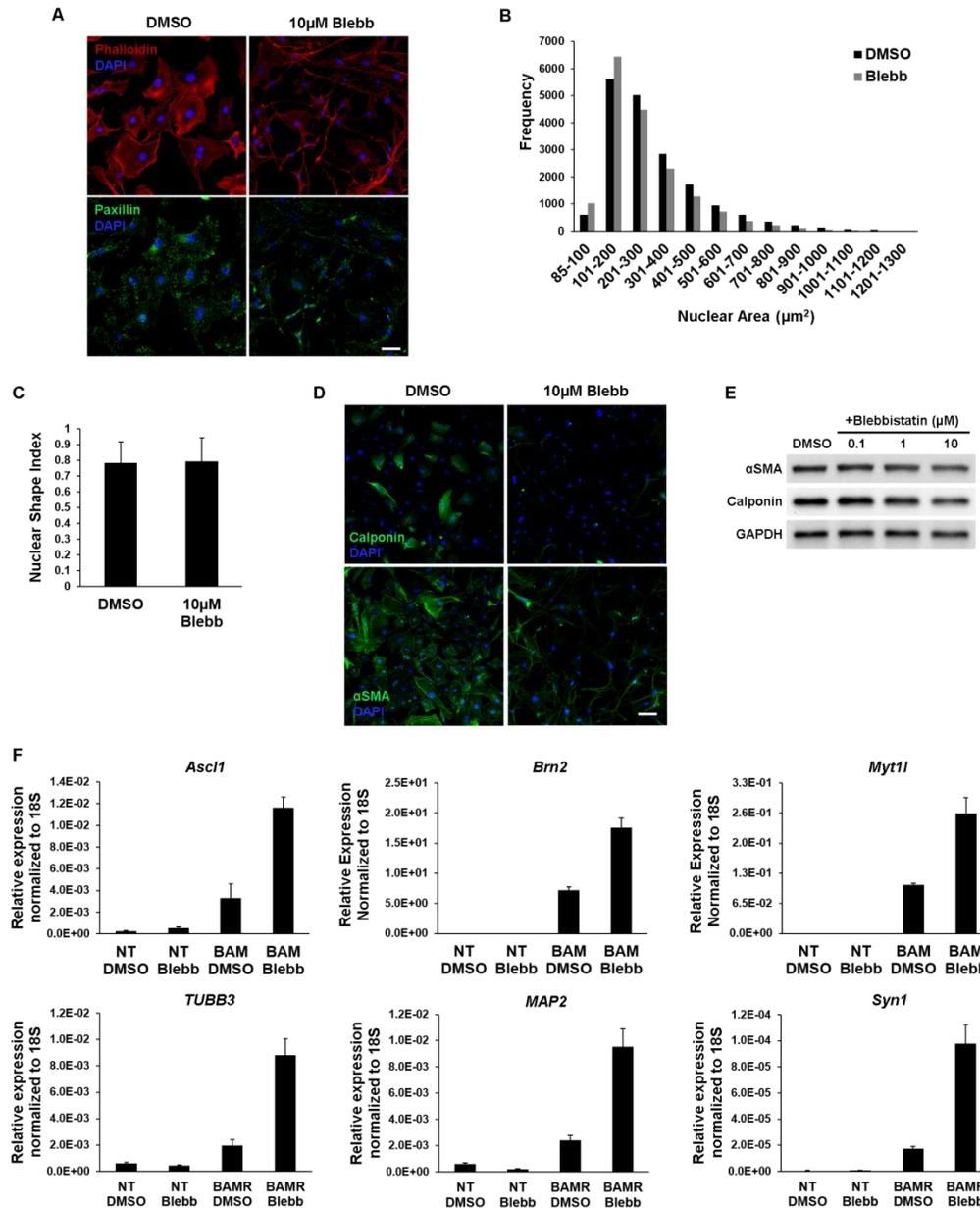
Figure 2.7 Blebbistatin induced cell morphological changes and regulated the expression of mesenchymal and neuronal markers. A-D. In these experiments, fibroblasts were treated with 10μM blebbistatin for 24 hours or 2 hours (**B-C**). **A.** Images show fluorescence micrograph of the actin network (phalloidin, red), focal adhesions (paxillin, green) and nucleus (DAPI, blue) (scale bar, 50 μm). **B-C.** Plots showing the effect of blebbistatin on nuclear area and shape. **D.** Immunofluorescent staining of calponin and αSMA in non-transduced fibroblasts (scale bar, 100 μm). **E.** BAM-transduced fibroblasts were treated with blebbistatin for 2 days, followed by Western blot analysis of mesenchymal markers, αSMA and calponin. GAPDH is shown as a loading control. **F.** qRT-PCR analysis of neuronal gene expression in non-transduced and BAM transduced fibroblasts cultured in the absence and presence of blebbistatin for 4 days (n=3).
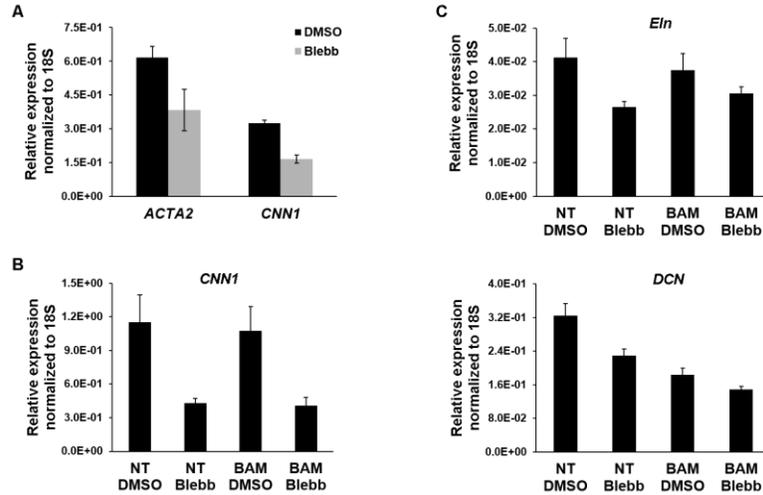
Figure 2.8 Blebbistatin downregulates mesenchymal gene expression. A. qRT-PCR analysis of *ACTA2* and *CNN1* expression in non-transduced fibroblasts treated with blebbistatin for 24 hours (n=3). **B.** qRT-PCR analysis of *CNN1* expression in non-transduced and BAM-transduced fibroblasts cultured in the absence and presence of blebbistatin for 2 days (n=3). **C.** Non-transduced and BAM-transduced fibroblasts treated with blebbistatin for 4 days followed by qRT-PCR analysis of fibroblast gene expression (n=3).
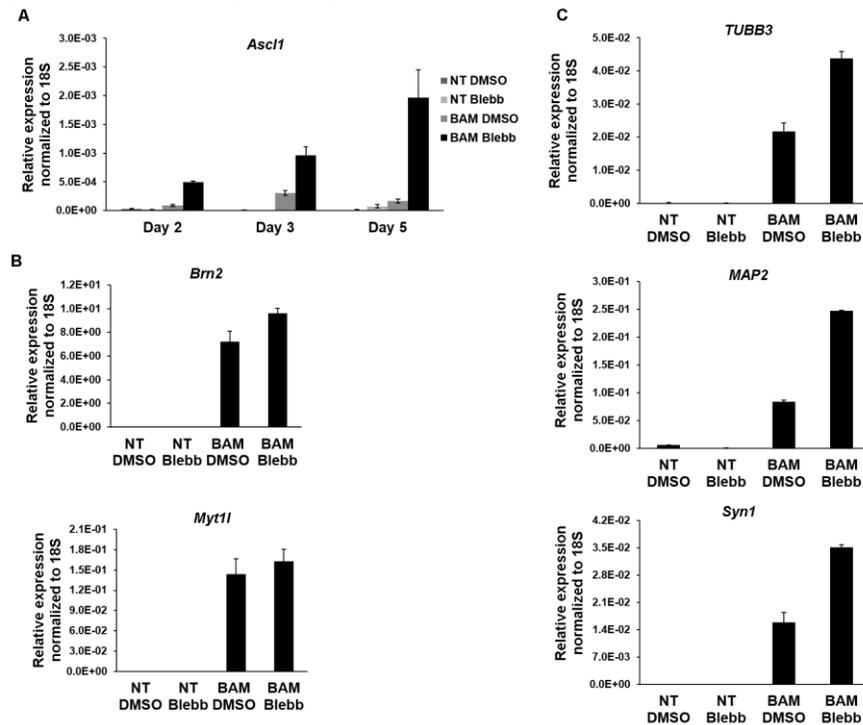
Figure 2.9 Neuronal gene expression is upregulated after blebbistatin treatment. A. Time course of *Ascl1* expression in non-transduced and BAM-transduced fibroblasts treated with and without blebbistatin (n=3). **B.** qRT-PCR analysis of *Brn2* and *Myt1l* expression on day 3 of BAM reprogramming (n=3). **C.** Non-transduced and BAM-transduced fibroblasts treated with and without blebbistatin were cultured for 14 days before performing qRT-PCR analysis of neuronal genes, *TUBB3*, *MAP2* and *Syn1* (n=3).

18
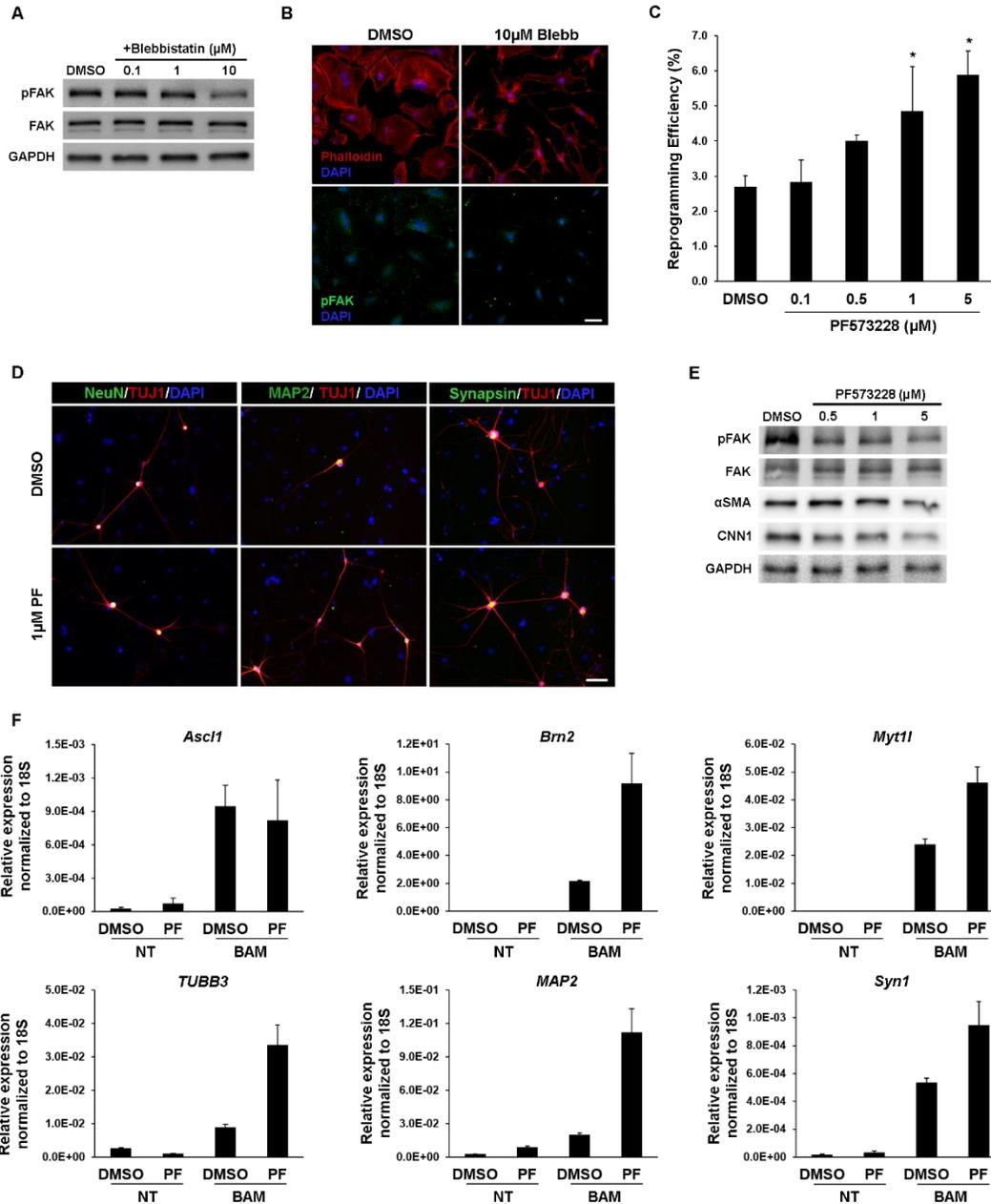
Figure 2.10 Focal adhesion kinase inhibition can improve iN cell generation. **A.** Western blot analysis of FAK expression in BAM transduced fibroblasts treated with varying concentrations of blebbistatin for 2 days. **B.** Non-transduced fibroblasts were treated with 10µM blebbistatin for 24 hours and then immunostained for phospho-FAK (pFAK). Top images show fluorescence micrographs of nucleus (DAPI, blue) and actin network (phalloidin, red). **C.** Reprogramming efficiency of fibroblasts transduced with BAM and cultured in the absence and presence of various concentrations of the FAK inhibitor, PF573228 (denoted as PF in this and the rest of the figures) (n=3) (*p<0.05). **D.** TUJ1+ iN cells derived in the presence of 1µM PF co-express mature neuronal markers and display a typical neuronal morphology. **E.** Western blot analysis of BAM-transduced fibroblasts that were treated with various concentrations of PF573228 for 2 days. **F.** qRT-PCR analysis of neuronal gene expression in non-transduced and BAM-transduced fibroblasts cultured in the absence and presence of 5µM PF573228 for 4 days (n=3).
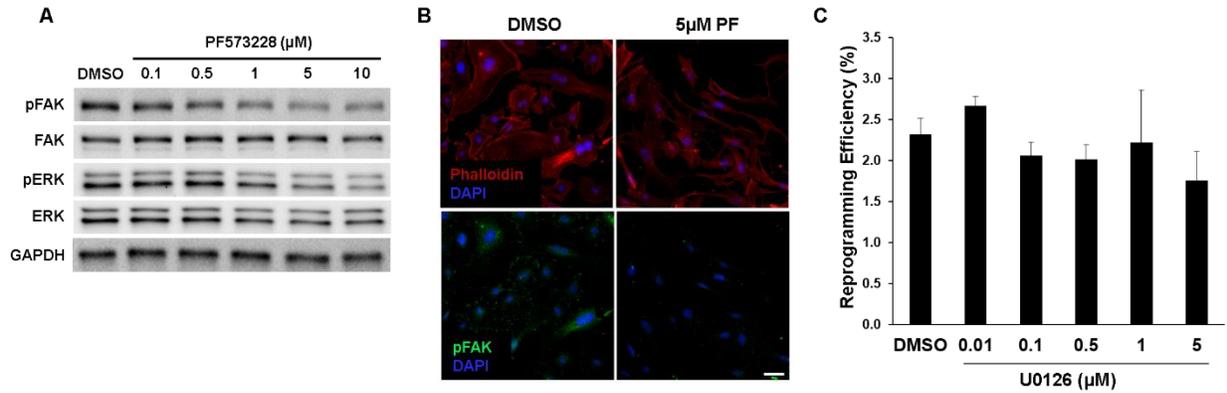
Figure 2.11 PF573228 specifically inhibits FAK activity. A. Western blot analysis of fibroblasts treated with varying doses of the FAK inhibitor, PF573228. PF573228 inhibits the phosphorylation of FAK and downstream ERK in a dose dependent manner. **B.** Immunofluorescence micrographs illustrate the cell morphology and expression of pFAK in fibroblasts treated with 5µM PF for 24 hours (scale bar, 50µm). **C.** Reprogramming efficiency of BAM-transduced fibroblasts treated with various concentrations of the ERK inhibitor, U0126 (n=3).
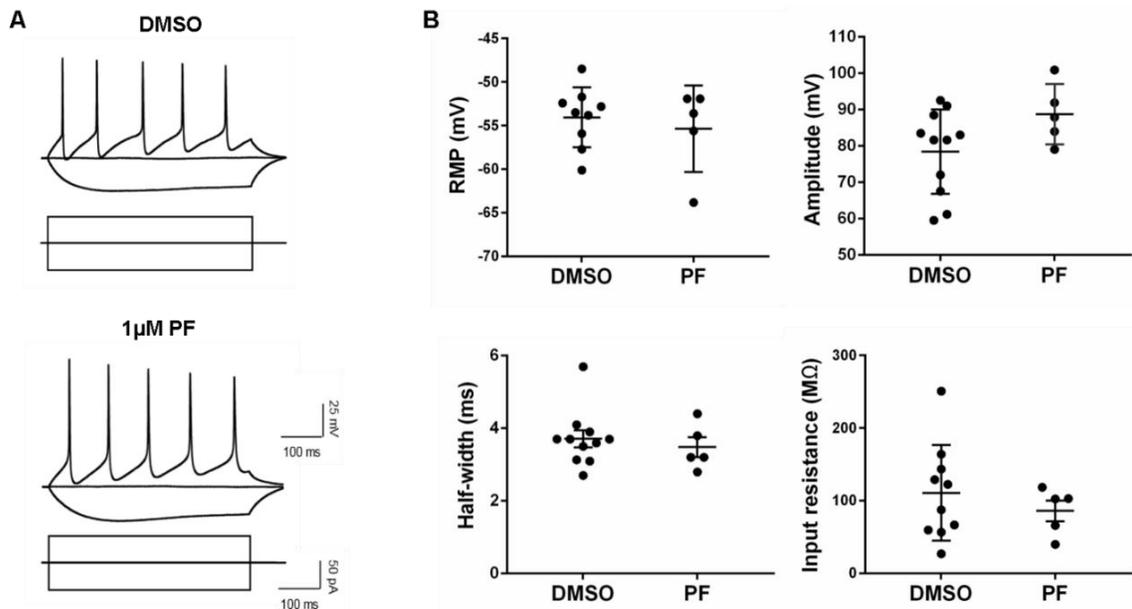
Figure 2.12 Electrophysiological analysis indicates functionality of PF573228-derived iN cells. A. Representative traces of spontaneous changes in membrane potential in response to current injection from iN cells obtained in the absence and presence of 1µM PF. PF573228 was administered during the first 7 days of reprogramming. **B.** Quantification of electrophysiological properties of iN cells. Each circle represents an individual cell that was tested. The resting membrane potential, RMP, input resistance and action potential amplitude and half-width were measured.

2.3.5 Role of Nuclear Membrane Proteins in Direct iN Conversion

It had been previously proposed that mechanical forces exerted at the cell surface might act a distance to elicit mechanochemical conversion in the nucleus[46]. Intriguingly, a recent study demonstrated that local stresses can be sensed by integrins, propagated through the actin cytoskeleton and transmitted across the nuclear lamina to stretch chromatin and upregulate transcription[47]. However, how the nuclear membrane might influence direct reprogramming remains unknown. Thus, we sought to understand blebbistatin's effect on nuclear membrane proteins and to elucidate their role in iN conversion.

First, we tested the effect of blebbistatin on the nuclear membrane protein lamin A/C. Immunostaining analysis showed that treatment with blebbistatin appeared to disrupt the nuclear lamina of fibroblasts, as indicated by lamin A/C staining (Figure 2.13A). To determine whether this nuclear membrane disruption played any role in direct reprogramming, fibroblasts isolated from wild-type (WT) and lamin A mutant mice were transduced with BAM and cultured in the absence and presence of 10μM blebbistatin. We observed that more iN cells were generated from lamin A mutant fibroblasts and moreover, there was synergistic enhancement in the conversion efficiency when lamin A mutant fibroblasts were induced to reprogram in the presence of blebbistatin (Figure 2.13B). Consistently, both WT- and lamin A mutant-derived iN cells expressed mature neuronal markers (Figure 2.13C).

Further examination of protein expression by Western blot analysis revealed that lamin mutant fibroblasts expressed lower levels of mesenchymal markers, αSMA and calponin, in comparison to wild-type cells (Figure 2.13D). Interestingly, the expression of these markers along with phospho-FAK were further reduced in the presence of blebbistatin. Additionally, we evaluated neuronal gene expression in non-transduced and BAM-transduced fibroblasts isolated from wild-type and lamin mutant mice and observed that certain neuronal genes, such as *Brn2*, *Myt1l* and *Syn1*, were highly expressed in the lamin mutant cells in comparison to the control (Figure 2.13E). When these same conditions were analyzed after treatment with blebbistatin, we found that blebbistatin increased the expression level of the neuronal genes tested and these were even further enhanced in the lamin mutant cells (Figure 2.13E).

Given we observed that blebbistatin could modulate the nuclear lamina to influence direct conversion, we then explored how emerin, another nuclear membrane protein, may be affected by cytoskeletal disruption. We found that blebbistatin altered the localization of emerin (Figure 2.14A). To elucidate the role of emerin in induced neuronal reprogramming, we used siRNA against emerin and confirmed knockdown of emerin at the gene and protein expression level (Figure 2.14 B-C). Compared to the negative control siRNA condition, we observed no apparent difference in the reprogramming efficiency of BAM-transduced fibroblasts cultured in the absence and presence of blebbistatin after siRNA knockdown of emerin (Figure 2.14D). In addition, we found that emerin silencing did not affect the expression of phospho-FAK, αSMA, and calponin. However, blebbistatin produced similar results in protein expression regardless of emerin knockdown (Figure 2.14E). This suggests that blebbistatin may induce these changes through a mechanism independent of emerin. Interestingly, BAM-transduced fibroblasts treated with blebbistatin after siRNA knockdown displayed the higher levels of neuronal gene expression compared to the other conditions (Figure 2.14F). Taken together, our data suggests that lamin A plays a more influential role on neuronal lineage conversion.
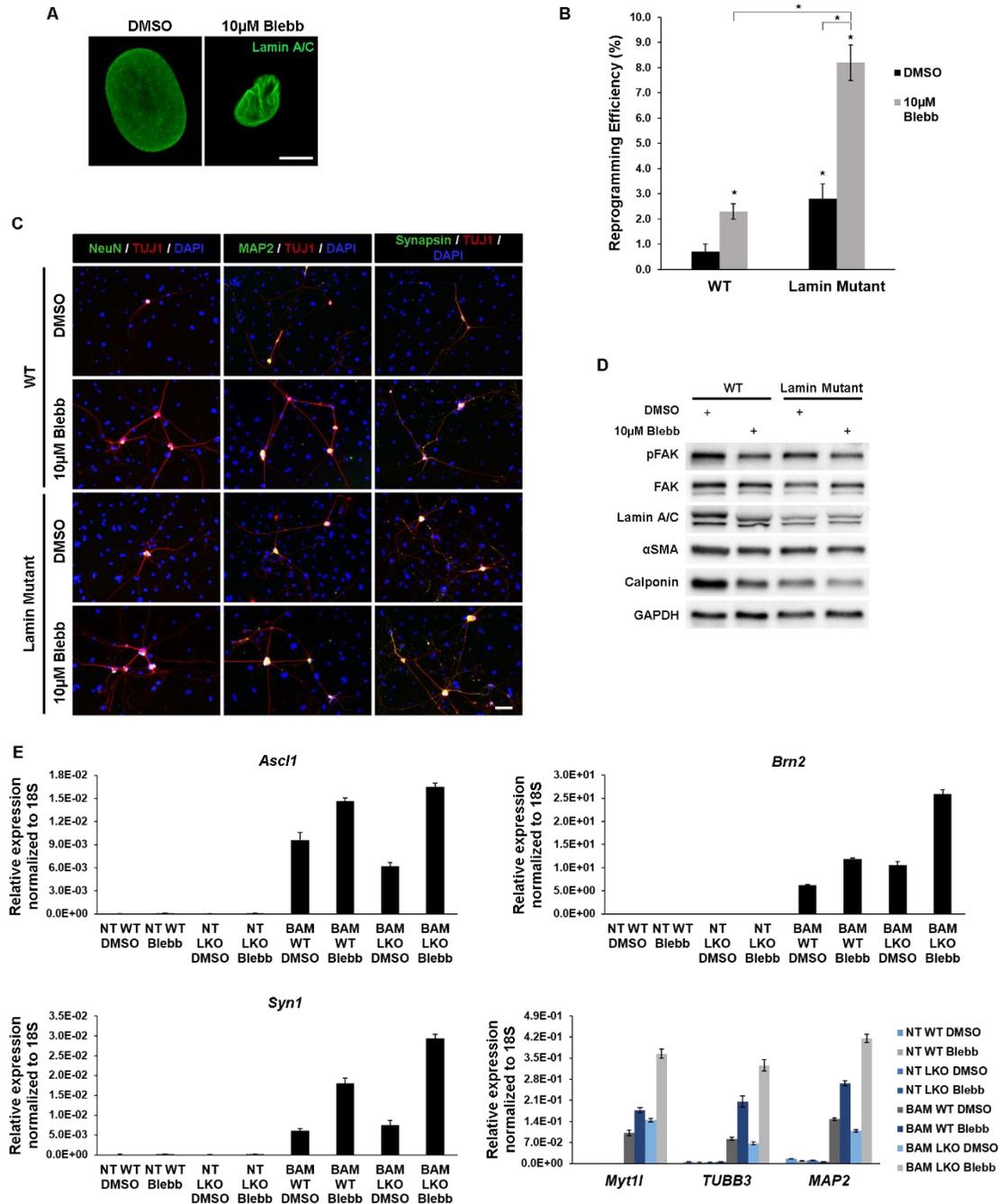
Figure 2.13 Disruption of lamin A influences the direct reprogramming fibroblasts into neurons. A. Fluorescence micrographs of lamin A/C in fibroblasts treated with 10μM blebbistatin for 2 hours (scale bar, 10μm). **B.** Reprogramming efficiency of wild-type and lamin mutant fibroblasts transduced with BAM and cultured in the absence and presence of blebbistatin (n=4) (*p<0.05). **C.** iN cells derived from wild-type and lamin mutant fibroblasts treated with blebbistatin express mature neuronal markers (scale bar, 100μm). **D.** Western blot analysis performed on wild-type and lamin mutant fibroblasts transduced with BAM and cultured in the absence and presence of blebbistatin for 2 days. **E.** Non-transduced and BAM-transduced fibroblasts from wild-type and lamin mutant mice were cultured with blebbistatin for 4 days, followed by qRT-PCR analysis of neuronal gene expression (n=3).
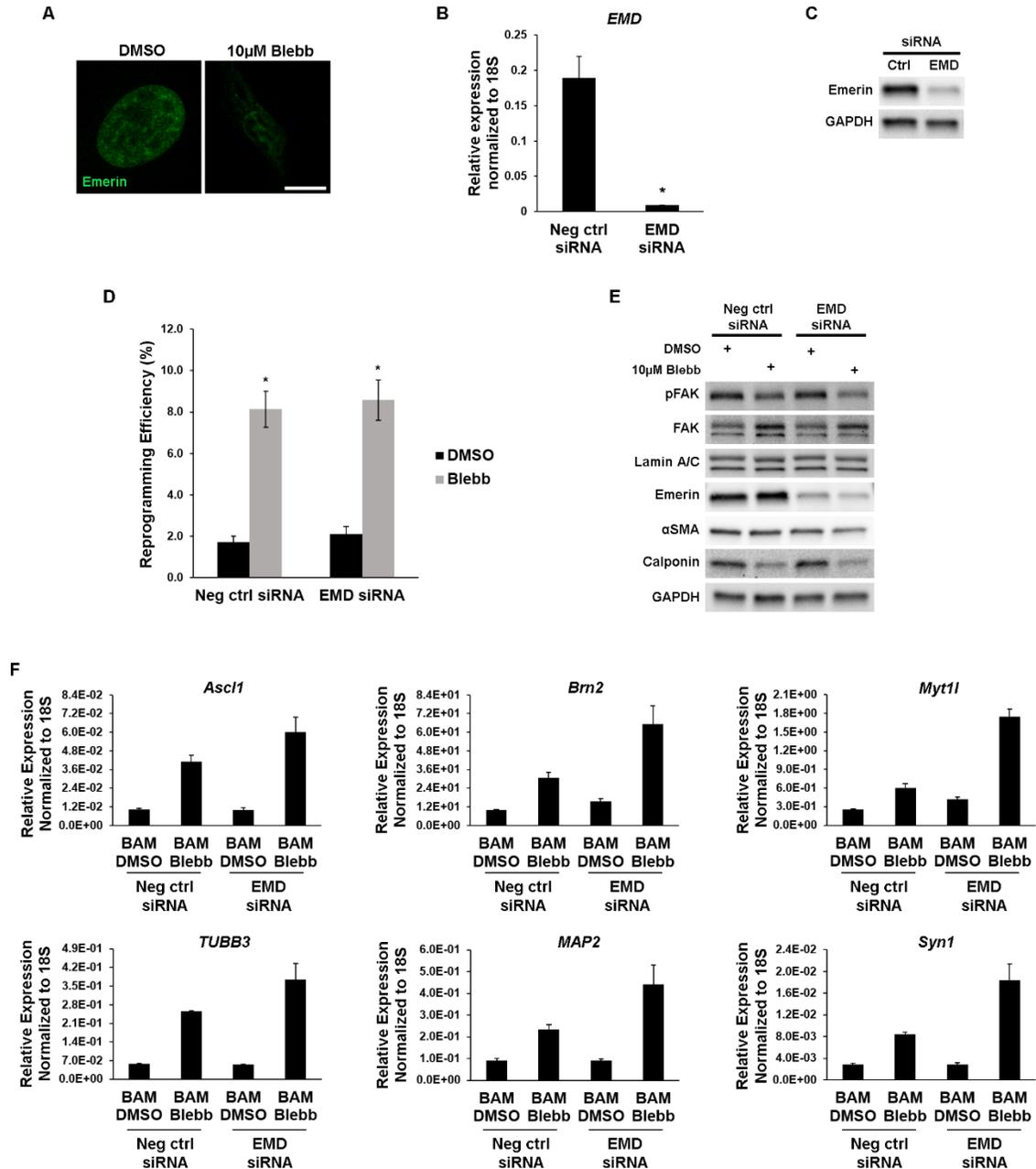
Figure 2.14 Effect of emerin knockdown on induced neuronal conversion. A. Immunofluorescence staining of emerin in fibroblasts treated with blebbistatin for 2 hours (scale bar, 10μm). **B.** qRT-PCR analysis confirms the knockdown of *EMD* expression in fibroblasts (n=3) (*p<0.05). **C.** Western blot analysis of emerin expression in fibroblasts after siRNA knockdown. **D.** Reprogramming efficiency of BAM-transduced fibroblasts cultured in the absence and presence of blebbistatin after siRNA knockdown of emerin (n=3) (*p<0.05). **E.** Western blot analysis performed on BAM-transduced fibroblasts treated with and without blebbistatin for 2 days after siRNA knockdown of *EMD*. **F.** qRT-PCR analysis of neuronal gene expression in BAM-transduced fibroblasts cultured with blebbistatin for 4 days after siRNA silencing of emerin (n=3).
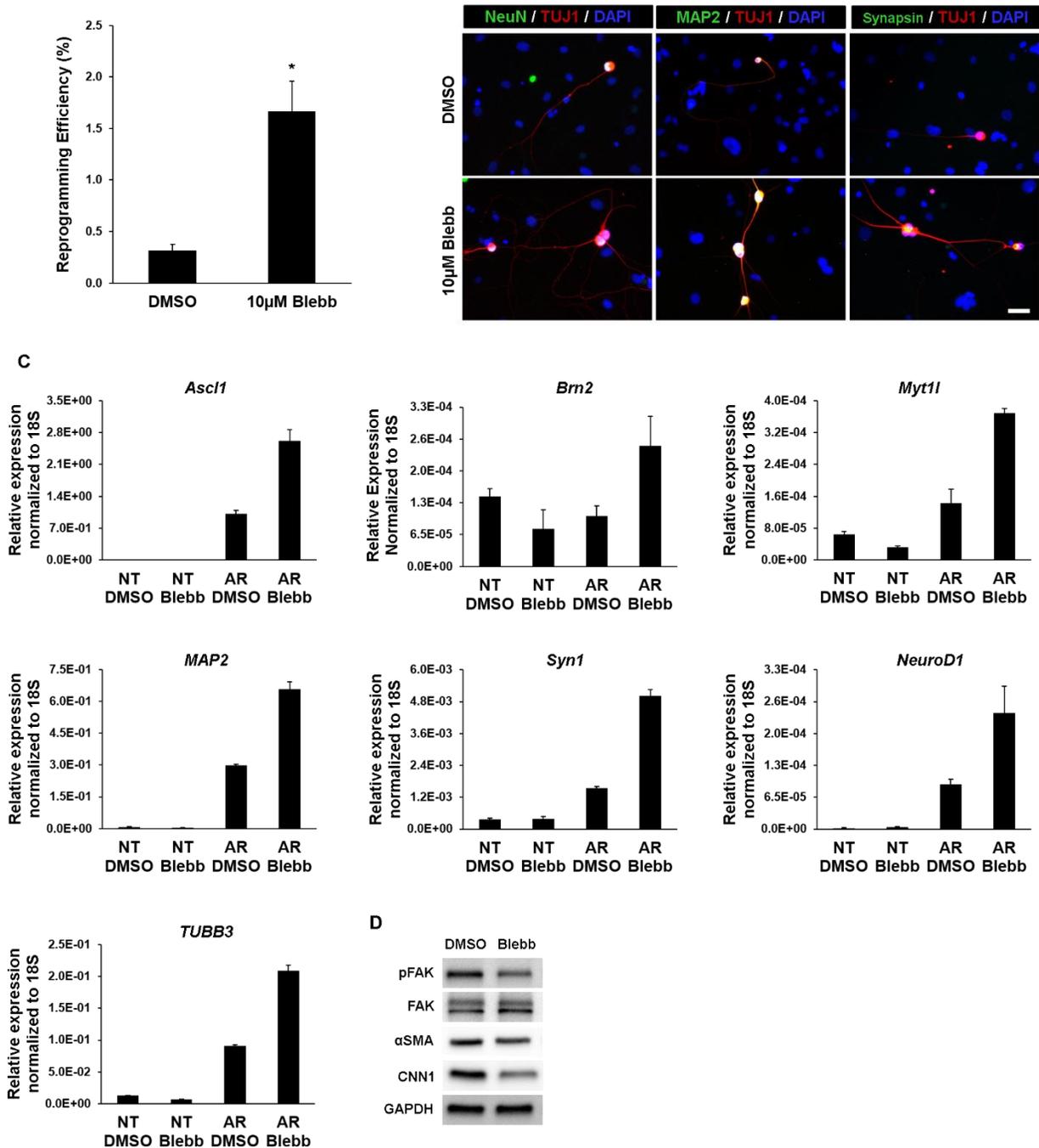
Figure 2.15 Blebbistatin can induce Brn2 and Myt1l expression to promote Ascl1 reprogramming. A. Reprogramming efficiency of fibroblasts transduced with Ascl1 and cultured in the absence and presence of 10μM blebbistatin (n=6) (*p<0.05). **B.** Fluorescence micrographs show co-expression of TUJ1 and mature neuronal markers in iN cells derived after Ascl1 transduction and treatment with blebbistatin (scale bar, 50μm). **C.** qRT-PCR analysis of neuronal gene expression in non-transduced and Ascl1-transduced fibroblasts cultured in the absence and presence of blebbistatin for 6 days (n=3). **D.** Western blot analysis of Ascl1-transduced fibroblasts treated with and without blebbistatin for 2 days.

2.3.6 Blebbistatin Promotes Ascl1 Reprogramming

Ascl1 has been identified as a pioneer factor that plays a critical role in the direct reprogramming of fibroblasts into induced neurons. It has been shown that Ascl1 is required for the initiation of iN conversion, as Brn2 and Myt1l reprogramming failed to produce iN cells, whereas Brn2 and Myt1l facilitate iN cell maturation[48]. Moreover, Ascl1 alone is sufficient to generate functional iN cells[49]. As blebbistatin modulated Ascl1 expression during BAM reprogramming, we were interested in investigating whether blebbistatin could influence the conversion of fibroblasts into neurons using a single factor. To test this, fibroblasts were transduced with Ascl1 alone and treated with and without 10μM blebbistatin for the first 7 days of reprogramming. Remarkably, we found that blebbistatin can generate significantly more iN cells compared to the control (Figure 2.15A). The TUJ1$^+$ iN cells were found to co-express NeuN, MAP2 and synapsin (Figure 2.15B). A similar trend was observed in the reprogramming efficiency of Tau-EGFP fibroblasts transduced with Ascl1 and cultured in the absence and presence of blebbistatin (Figure 2.16).

We then sought to understand how blebbistatin could modulate the conversion efficiency in Ascl1 reprogramming. Considering two additional transcription factors along with Ascl1 are included in the reprogramming cocktail to generate induced neurons, we questioned if perhaps blebbistatin can induce the expression of Brn2 and Myt1l to promote single factor reprogramming. Utilizing qRT-PCR to analyze changes in neuronal gene expression in Ascl1-transduced fibroblasts, we observed that blebbistatin upregulated the expression of endogenous Brn2 and Myt1l (Figure 2.15C). Moreover, the expression of several neuronal genes, including the master neuronal gene, *NeuroD1*, was also higher in Ascl1-transduced fibroblasts treated with blebbistatin (Figure 2.15C). Consistent with our previous results, blebbistatin was able to decrease the expression of phospho-FAK, αSMA and calponin in Ascl1-transduced fibroblasts (Figure 2.15D). In summary, our findings demonstrate that blebbistatin can induce the expression of key neuronal genes to promote Ascl1-mediated iN conversion. The effects of blebbistatin on induced neuronal reprogramming are summarized in Figure 2.17.
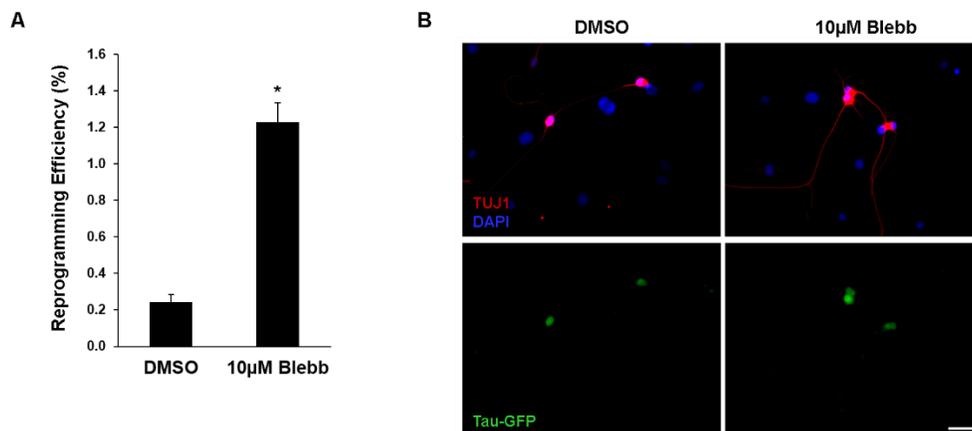
Figure 2.16 Blebbistatin enhances the reprogramming efficiency of Ascl1-transduced Tau-EGFP fibroblasts. A. Reprogramming efficiency of Tau-EGFP fibroblasts transduced with Ascl1 and cultured in the absence and presence of 10μM blebbistatin (n=6) (*p<0.05). **B.** Immunofluorescent images of Tau-EGFP derived-iN cells expressing TUJ1 and Tau-GFP (scale bar, 50μm).
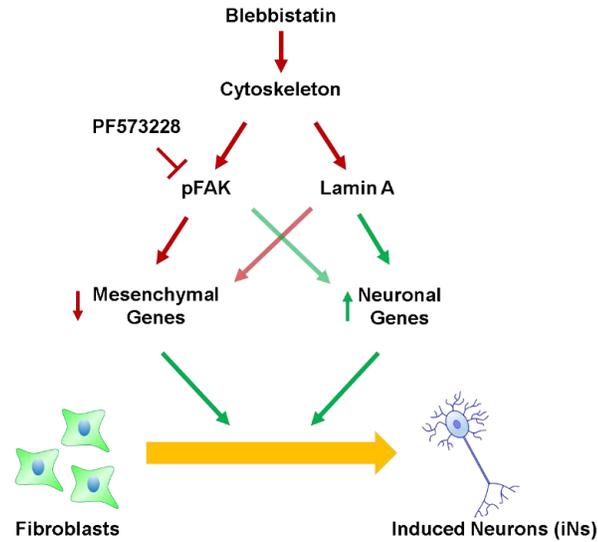
Figure 2.17 Hypothesis of the effects of blebbistatin on the direct reprogramming of adult mouse fibroblasts into neurons.

In conclusion, findings from this study demonstrate, for the first time, the role of the cytoskeleton and nucleoskeleton in the direct reprogramming of fibroblasts into neurons. We found that inhibition of myosin II using blebbistatin can influence the conversion efficiency. This direct relationship between the conversion efficiency and the concentration of the inhibitor was also apparent when using the ROCK inhibitor, Y-27632, and PF573228, a FAK inhibitor, respectively. We reveal that the blebbistatin-induced enhancement in the efficiency may be attributed to the inhibition of focal adhesion kinase signaling and alterations in the nuclear lamina. Moreover, this study shows that blebbistatin can regulate gene expression to modulate iN conversion. Altogether, these findings highlight how biochemical cues can be used to improve the conversion efficiency and have important implications for neurological disease modeling and regenerative medicine.

Chapter 3: Effect of Topography on Direct Reprogramming of Fibroblasts into Neurons

3.1 Introduction

Neurodegenerative disorders that result in the loss of nerve cells are currently on the rise in our aging population[50,51]. As result, there is a need to gain a better understanding of the causes of disease in order to develop improved treatments and potential cures as these disorders are often incurable. Direct reprogramming, the process by which a mature cell is converted into a different cell type while omitting a pluripotent state, offers to be a promising approach for such debilitating conditions.

In 2010, Vierbuchen *et al.* introduced how it was possible to convert mouse embryonic and postnatal tail-tip fibroblasts into neurons via the forced expression of three transcription factors: *Ascl1*, *Brn2* and *Myt1l* (BAM)[4]. They demonstrated that these induced neuronal (iN) cells expressed neuronal markers, displayed complex neuronal morphologies, and exhibited functional neuronal properties. The reproducibility of this system has been further demonstrated as multiple groups have reported how different combinations of transcription factors and microRNAs can be used to yield neurons, in some cases specific neuronal subtypes, from fibroblasts[30,31,33,52–55]. Similarly, this process has also been applied to human fibroblasts[56]. However, human iN conversion efficiency remains quite low and thus its potential use for clinical applications is limited as neurons cannot proliferate. Additionally, direct reprogramming strategies can be used for drug screening and to model disease progression as it has been shown that induced neurons from fibroblasts isolated from patients with familial Alzheimer's disease can recapitulate hallmarks of the disease[53]. More recently, it has been shown that the exogenous use of transcription factors can be replaced using only small molecule compounds to directly convert fibroblasts into neurons[16,17].

Biophysical factors (i.e. topographical and mechanical properties of cell-adhesive substrates) have been shown to regulate many cell processes. In particular, there are many reports illustrating how topography can influence various cellular behaviors, such as cell shape[19,20], cell polarity[57], migration[23], proliferation[21] and the differentiation potential of stem cells[28,58,59,60,61]. Recently, our lab has shown for the first time that biophysical cues, in the form of parallel microgrooves on the surface of cell-adhesive substrates, can regulate the cell epigenetic state and significantly improve the reprogramming of fibroblasts into induced pluripotent stem cells (iPSCs)[62]. We were able to generalize the role of topography in this epigenetic mechanomodulation through the use of nanofibrous membranes. As with microgrooves, we found that aligned nanofibers were able to induce changes in epigenetic modifications and significantly enhanced the reprogramming efficiency, confirming through micro-island patterning that it was the changes in cell morphology that modulated the epigenetic state. However, despite the extensive literature of how cell behavior is regulated by topographical cues, the role of topography in the direct reprogramming process is less understood.

The purpose of this study was to elucidate whether topographical guidance can influence the direct conversion of fibroblasts to neurons, utilizing reprogramming technology in conjunction with various bioengineered substrates. Here, we report the effects of micro- and nanotopography on induced neuronal conversion, suggesting that biophysical factors, in the form of topographical cues, can modulate the direct reprogramming process.

3.2 Materials and Methods

3.2.1 Fabrication and Preparation of Cell Adhesive Substrates

Fabrication of microgrooves and nanofiber substrates

Bioengineered substrates were fabricated as previously described[23,63,64]. Briefly, polydimethylsiloxane (PDMS) membranes were manufactured using well established soft lithography procedures. Poly(L-lactide-co-caprolactone) nanofibrous membranes were fabricated with either a random or aligned fiber orientation using electrospinning technology, where random fibers were ejected onto a grounded collector and aligned fibers were produced by performing certain collector modifications or mechanical stretch. For both cases, the nanofibers were collected on a polycarbonate (PC) membrane. Substrates were coated with laminin overnight, unless otherwise stated.

3.2.2 Fibroblast Isolation, Culture, and Reprogramming

Fibroblast isolation, culture, and reprogramming

Ear tissues from adult B57BL/6 mice were isolated, minced and partially digested in Liberase™ (0.025mg/ml, Roche) for 45 minutes under constant agitation at 37°C. Partially digested tissues were plated and fibroblasts were allowed to migrate out (passage 0). Isolated fibroblasts were expanded in MEF medium (DMEM+10% FBS [Corning] and 1% penicillin/streptomycin [GIBCO]) and used at passage 2 for all experiments. Fibroblasts from Tau-GFP reporter mice (004779; The Jackson Laboratory) were isolated as described above. Normal neonatal human dermal fibroblasts (nHDF) were purchased from Lonza (CC-2509) and expanded in FGM™-2 BulletKit™ (CC-3132) for 1-2 passages.

After transduction, mouse fibroblasts were seeded onto PDMS or nanofiber substrates and tissue culture-treated polystyrene (TCPS) dishes (Falcon) coated with Laminin (0.1mg/ml, Corning). Twenty-four hours after seeding the medium was replaced to MEF medium containing doxycycline (2μg/ml, Sigma). The following day the medium was changed to N3 medium (DMEM/F12 [GIBCO] + N2 supplement [Invitrogen] + B27 supplement [Invitrogen] + 1% penicillin/streptomycin [Gibco] + doxycycline [2μg/ml, Sigma]) and the cultures were maintained in this medium for the duration of the experiments. For Ascl1-only reprogramming, N3 medium was further supplemented with BDNF (5ng/ml, R&D systems) and GDNF (5ng/ml, R&D systems) after day 7. Reprogrammed nHDF were cultured in N3 medium without penicillin/streptomycin. Culture medium was replenished every 2-3 days during reprogramming. After reprogramming for the desired length (14 days for BAM, 21 days for Ascl1 only, and 28 days for human), the induced neuronal cells were analyzed and the reprogramming efficiency was determined.

Lentiviral production and cell transduction

Doxycycline-inducible lentiviral vectors for Tet-O-FUW-Ascl1, Tet-O-FUW-Brn2, Tet-O-FUW-Myt1l, FUW-rtTA, and Tet-O-FUW-NeuroD1 plasmids were used to transduce fibroblasts for

ectopic expression of rtTA, Brn2, Ascl1, Myt1l and NeuroD1. Lentivirus was made using established calcium phosphate transfection methods. Viral particles were collected and concentrated using Lenti-X Concentrator (Clontech) according to the manufacturer's protocol. Stable virus was aliquoted and stored at -80°C. For viral transduction, fibroblasts were seeded and allowed to attach overnight before incubation with virus and polybrene (8µg/ml, Sigma) for 24 hours. After incubation, transduced cells were reseeded onto laminin-coated bioengineered substrates (PDMS membranes or nanofibers) and TCPS dishes.

3.2.3 Induced Neuronal Characterization and Functional Assessment

Immunofluorescent staining and quantification

For immunostaining, cells were fixed with 4% paraformaldehyde, permeabilized with 0.5% Triton-X-100 (Sigma), and blocked with 5% donkey serum (Jackson Immunoresearch) in phosphate buffered saline (PBS). For actin-cytoskeleton staining, samples were incubated with fluorescein isothiocyanate-conjugated phalloidin (Invitrogen) for 1 hour. Primary antibodies were incubated overnight at 4°C, followed by 1-hour incubation with Alexa 488 and/or Alexa 546 -labeled secondary antibodies (Molecular Probes). Nuclei were stained with 4,6-diamino-2-phenylindole (DAPI) (Invitrogen). Refer to Table 3.1 for all antibody information.

Two to four weeks after the addition of doxycycline, cultures were fixed and immunostained for neuronal beta-III tubulin (TUJ1). Induced neuronal cells were quantified using a Zeiss Axio Observer.D1 and identified based on displays of a typical neuronal morphology (defined as cells with a circular cell body containing a neurite that is at least three times the length of the cell body) and positive TUJ1 expression. The reprogramming efficiency was determined by quantifying the total number of TUJ1$^+$ iN cells in each condition and normalizing it to the number of cells present at 24 hours post-seeding. Epifluorescence images were collected using a Zeiss Axio Observer.D1 whereas confocal images were collected using a Zeiss LSM710 microscope.

Table 3.1 Antibody information for immunofluorescent staining analysis

Antibody	Vendor	Catalog #	Dilution	Application
Tuj1	Covance	MMS435P	1:1000	IF
Tuj1	Covance	MRB435P	1:1000	IF
NeuN	Covance	SIG39860	1:100	IF
MAP2	Sigma	M9942	1:200	IF
Synapsin	Abcam	ab64581	1:200	IF
VGlut1	Millipore	MAB5502	1:200	IF
GABA	Sigma	A2052	1:500	IF

Electrophysiology

All experiments were conducted at room temperature (22°C–24°C). All reagents were purchased from Sigma-Aldrich unless specified otherwise. Whole-cell recording was made from neurons using a patch clamp amplifier (MultiClamp 700B, Axon Instr.) under infrared differential interference contrast optics. Microelectrodes were made from borosilicate glass capillaries, with a resistance of 4–5 MW. For recording action potentials, cells were held at −70 mV in a voltage-clamp mode. The intracellular solution for whole-cell recording of EPSPs and action potentials contained (in mM) 140 potassium gluconate, 5 KCl, 10 HEPES, 0.2 EGTA, 2 $MgCl_2$, 4 MgATP, 0.3 Na_2GTP and 10 Na_2-phosphocreatine, pH 7.2 (adjusted with KOH).

Off-line analyses of action potential properties (number, amplitude, half-width) were performed by using a threshold event detection function of Clampfit software (Molecular Devices). Visualization of analysis results and their statistical tests were performed by using GraphPad Prism® 6.0 software.

3.2.4 Biochemical Analysis of Gene Expression

qRT-PCR

RNA was isolated from samples using Trizol® (Ambion) according to the manufacturer's instructions. For cDNA synthesis, 500 ng of RNA was reverse transcribed using Maxima First Strand cDNA Synthesis Kit (Thermo). Template DNA was amplified using Maxima SYBR Green/Fluorescein qPCR Master Mix (Thermo) on a CFX qPCR machine (Bio-Rad). qRT-PCR data were analyzed using CFX Manager 3.1 (Bio-Rad) and gene expression levels were normalized to 18S. Primers used for qRT-PCR are included in Table 3.2.

Statistical Analysis

The data are presented as mean $\pm$ one standard deviation. Comparisons among values for groups greater than two were performed using a one-way analysis of variance (ANOVA) followed by a Tukey's post-hoc test to assess differences between the groups. For comparison between two groups, a two-tailed, unpaired t-test was used. For all cases, p-values less than 0.05 were considered statistically significant. GraphPad Prism® 6.0 software was used for all statistical evaluations.

Table 3.2 Primers used in qRT-PCR analysis

Gene Name	Forward Primer	Reverse Primer
Ascl1	GAAGCAGGATGGCAGCAGAT	TTTTCTGCCTCCCCATTTGA
Brn2	AGGGCGCAAACGGAAAA	GGCTTAGGGCATTTGAGGAAA
Myt1l	CTACAAGATGGACGTGGACTCTGA	GGAACTCGAACCCCTTTGG
TUBB3	GCGCCTTTGGACACCTATTC	CACCACTCTGACCAAAGATAAAGTTGT
18S	GCCGCTAGAGGTGAAATTCTTG	CATTCTTGGCAAATGCTTTCG

3.3 Results and Discussion

3.3.1 The Effect of Microtopographical Cues on Induced Neuronal Reprogramming

To elucidate the effect of topography on induced neuronal reprogramming, adult mouse fibroblasts were transduced with doxycycline-inducible lentiviral vectors encoding the three key reprogramming factors, *Brn2*, *Ascl1*, and *Myt1l* (BAM). Twenty four hours after transduction, cells were seeded onto flat poly(dimethyl siloxane) (PDMS) membranes or those fabricated with parallel microgrooves of various width and spacing and tissue culture polystyrene (TCPS) dishes coated with same extracellular matrix (ECM) protein. The groove heights were maintained at 3 μm for all cases. As depicted in Figure 3.1A, the cultures were maintained in neuronal culture conditions for 14 days at which point the cells were fixed and immunostained for neuronal β-III tubulin (TUJ1) and the reprogramming efficiency was determined. Induced neuronal (iN) cells were identified based on displays of a typical neuronal morphology (defined as cells with a circular soma extending processes that are at least three times the length of the cell body) and TUJ1 expression. Induced neuronal cells were observed on all the substrates. Interestingly, the iN cells derived the microgrooves favored neurite outgrowth along the axis of groove alignment (Figure 3.1B). Additionally, we observed that microtopography was only able to moderately increase the reprogramming efficiency, as microgrooves with 10 μm width and spacing generated the highest efficiency (Figure 3.1C). As a result, 10 μm microgrooves were used in all the remaining experiments. Although microgrooves did not significantly enhance the efficiency compared to the flat membranes, PDMS membranes, as a whole, were able to improve the yield of iN cells compared to the TCPS condition (Figure 3.1C).

Furthermore, we observed a similar trend in the reprogramming efficiency across the various substrates regardless of the ECM protein coated on the surface (Figure 3.1D). Although Matrigel and laminin were able to yield the highest efficiencies, Matrigel is associated with batch-to-batch variations and thus, laminin was used in all further studies. This finding is supported by literature, which has shown that laminin is important during the development of the nervous system and can promote neurite outgrowth[65–67]. Consistently, we also observed a similar trend in the reprogramming efficiency of neonatal human dermal fibroblasts (nHDF) transduced with BAM plus NeuroD1 and cultured on flat or grooved PDMS substrates and TCPS (Figure 3.2).
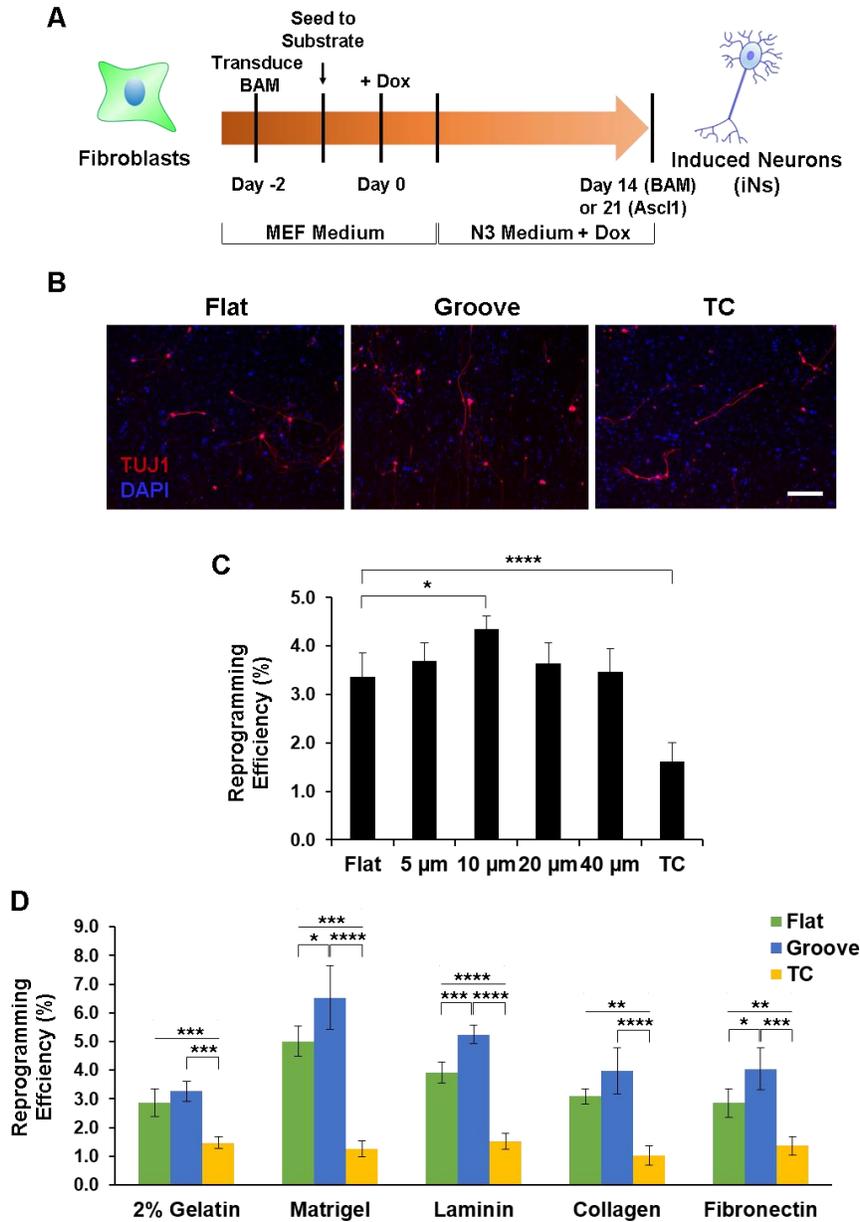
Figure 3.1 Microtopographical cues modestly influence induced neuronal reprogramming.
A. Reprogramming protocol for converting adult mouse fibroblasts into neurons using the reprogramming factors- *Brn2*, *Ascl1* and *Myt1l* (BAM). Cells were cultured in N3 medium for 14 days before immunostaining and quantification. **B.** Representative fluorescent micrographs of iNs expressing TUJ1 after being generated on flat and 10µm microgrooved PDMS membranes and tissue culture polystyrene (TCPS, denoted as TC in this and all the figures). **C.** Reprogramming efficiency of fibroblasts transduced with BAM and cultured on flat and grooved PDMS membranes with various width and spacing and TCPS. The number of biological replicates, n, was equal to 4 for this experiment. **D.** Reprogramming efficiency of BAM-transduced fibroblasts cultured on flat and grooved PDMS membranes and TCPS coated with various ECM proteins (n=4). Microgrooved substrates with 10µm width and spacing, denoted as "Groove" in this and the rest of the figures, were used for the experiments. In all the figures, statistical significant differences are denoted as *, where $p < 0.05$.
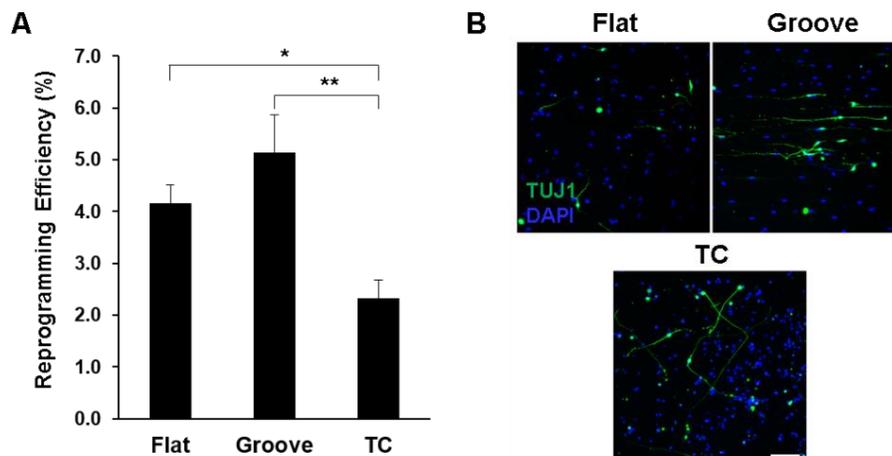
Figure 3.2 Effect of microtopography on human induced neuronal reprogramming.
A. Reprogramming efficiency of neonatal human dermal fibroblasts (nHDF) transduced with BAM along with NeuroD1 and cultured on flat and grooved PDMS membranes and TCPS (n=4) (*p<0.05). **B.** Representative fluorescent micrographs of nHDF-derived iNs expressing TUJ1 after being generated on the various surfaces (scale bar, 100μm).

3.3.2 Characterization of Topography-derived iN Cells

After observing that microtopographical cues could influence iN conversion efficiency, we then assessed the maturation and functionality of the derived iN cells. We found that the iN cells exhibited positive staining for neuronal markers, MAP2 (microtubule-associated protein 2) and NeuN (Figure 3.3A and data not shown). Additionally, we determined that the iN cells displayed a GABAergic phenotype (Figure 3.3A). iN cells were then subjected to whole-cell patch clamp to determine their functionality. We observed that iN cells derived on flat PDMS membranes and TCPS were functional as they were able to generate action potentials upon depolarization of the membrane in current clamp mode (Figure 3.3B). Further analysis showed that there were no apparent differences in other electrophysiological characteristics of iNs generated on both surfaces (Figure 3.3C-G). Altogether, this data suggests that the derived iN cells are mature and functional.
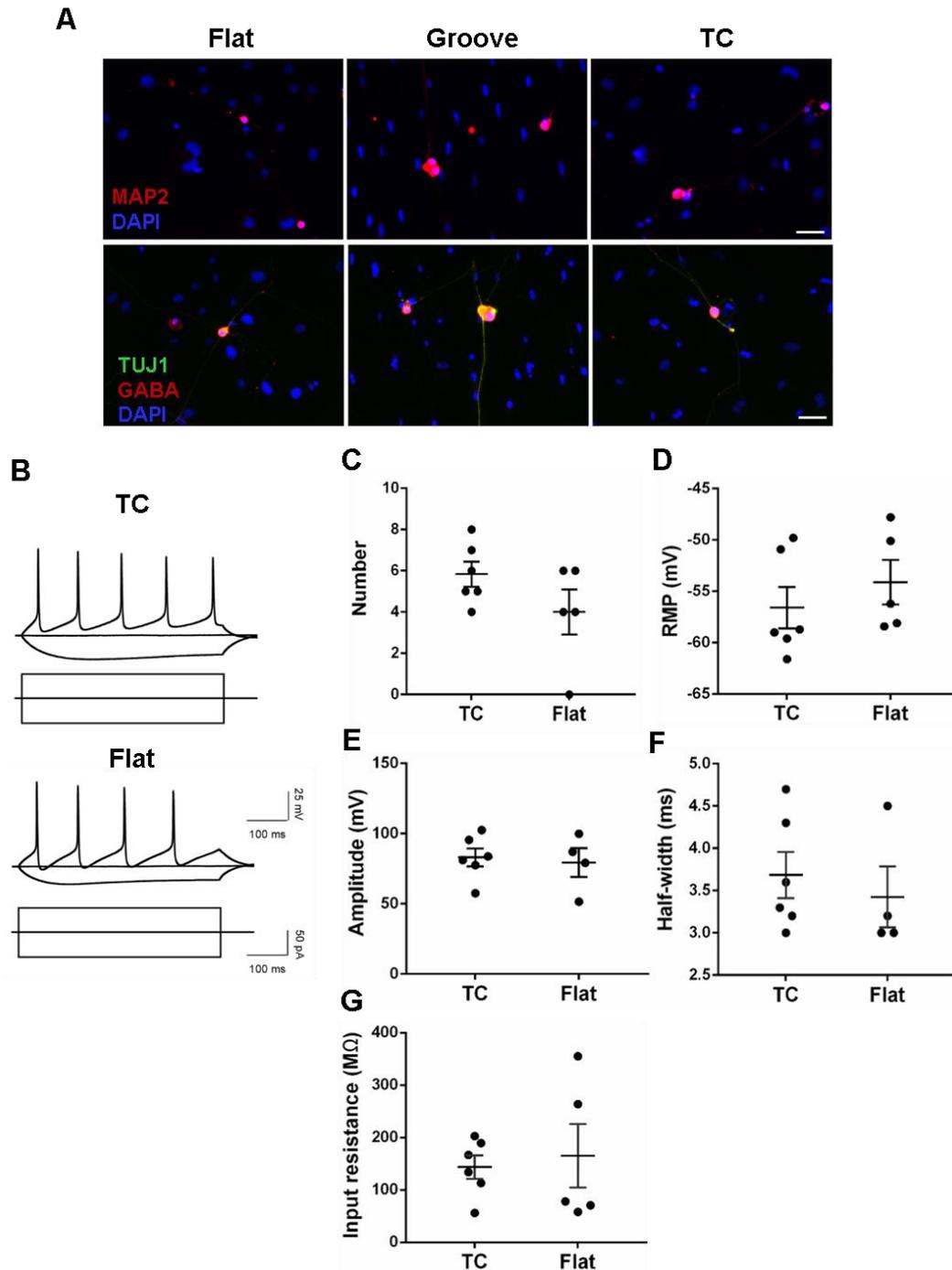
Figure 3.3 iN cells express neuronal markers and display functional neuronal properties. A. Representative fluorescent images of iN cells expressing the mature neuronal marker, MAP2, and co-expressing TUJ1 and GABA (scale bar, 50µm). **B.** Representative traces of spontaneous changes in membrane potential in response to current injection from iNs obtained on TC and flat PDMS membranes. **C-G.** Quantification of electrophysiological properties of iN cells. Each circle represents an individual cell that was tested. The number of action potentials (C), resting membrane potential, RMP (D), action potential amplitude (E) and half-width (F) as well as input resistance (G) were measured. Graphs show the mean $\pm$ one standard error of mean.
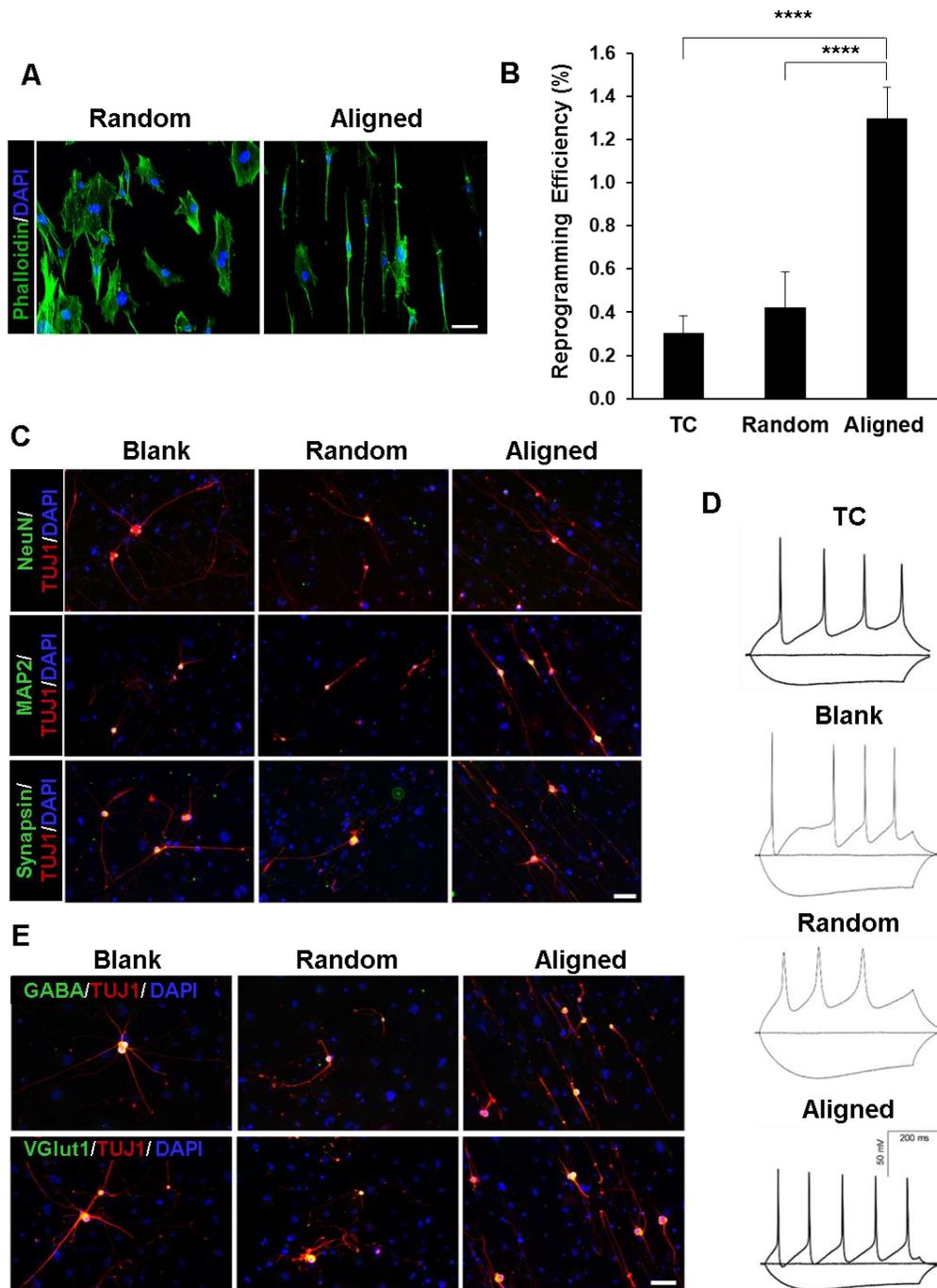
Figure 3.4 Nanofiber alignment enhances the efficiency of iN conversion. A. Confocal fluorescence micrographs of mouse fibroblasts cultured on nanofibers. Images show the actin network (phalloidin, green) and nucleus (DAPI, blue) (scale bar, 50 µm). **B.** Reprogramming efficiency of BAM-transduced mouse fibroblasts cultured on TCPS and nanofibers with random or aligned fiber orientation (n=2) (*p<0.05). **C.** Representative fluorescent images of TUJ1+ iNs cells co-expressing mature neuronal markers, NeuN, MAP2, and synapsin (scale bar, 100µm). **D.** Representative traces of spontaneous changes in membrane potential in response to current injection from iNs obtained on the various surfaces. **E.** Immunofluorescent images of TUJ1^{+} iNs expressing GABA and VGlut1 (scale bar, 100µm).

3.3.3 Nanofiber Alignment Improves the Yield of Mature, Functional iN Cells

Nanotopography can regulate various cell functions, including cell shape[19,20], cell polarity[57], and migration[23]. Its role can be further extended into cell reprogramming as recent work from our lab has shown that aligned nanofibrous scaffolds can enhance iPSC reprogramming efficiency [62]. In addition, other studies have reported that anisotropic patterns and aligned fibrous substrates can enhance neuronal marker expression, guide neurite outgrowth and promote neuronal differentiation of stem cells[28,58,68,69,70]. Thus, we set out to explore the role of nanotopography in the direct conversion of fibroblasts into neurons with the use of nanofibrous membranes.

Upon seeding mouse fibroblasts onto electrospun nanofibrous membranes with either a random or aligned fiber orientation, we observed that the cell morphology was altered. Aligned nanofibers encouraged fibroblast alignment and elongation over random nanofibers and decreased cell spreading (Figure 3.4A). Next, we seeded fibroblasts transduced with BAM onto nanofiber surfaces, TCPS, and in some cases, a "blank" polycarbonate (PC) membrane that had no fibers and served as an additional control in order to test the effects of fiber orientation on the reprogramming efficiency. We found that we were able to generate iN cells in all the conditions tested and aligned nanofibers promoted and guided neurite outgrowth. Interestingly, aligned nanofibers were more efficient at converting fibroblasts into neurons in comparison to random nanofibers and TCPS (Figure 3.4B). Aligned nanofibers enhanced the conversion efficiency by approximately 3-fold. Although to a lesser extent, a similar trend in the efficiency was observed in mouse fibroblasts isolated from Tau-EGFP mice, whereby cells expressing the neuronal marker, Tau, are concomitantly labeled with GFP (Figure 3.5).

Further characterization of the iN cells generated on the nanotopographical sufaces revealed that the cells expressed mature neuronal markers, including NeuN, MAP2, and synapsin (Figure 3.4C). Electrophysiological analysis indicated that the induced neurons were functional, exhibiting spontaneous changes in membrane potential in response to current injection (Figure 3.4D). Although there were no significant differences in the number of action potentials that were generated across the various groups, certain action potential properties seemed to be affected (Figure 3.6A-C). For example, the action potential amplitude of iN cells generated on aligned nanofibers was significantly higher than random nanofibers and TCPS, suggesting that topographical cues may influence some neuronal properties of iN cells. Conversely, other electrophysiological properties, such as the resting membrane potential (RMP) and input resistance, appeared to be similar among the various surfaces (Figure 3.6D-E). Furthermore, iN cells were found to be of the GABAergic and glutamatergic neuronal subtypes (Figure 3.4E). In summary, aligned nanofibers can enhance the conversion efficiency to produce mature, functional iN cells.
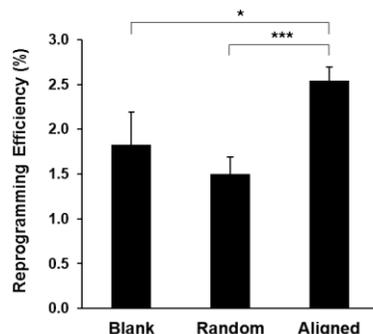

Figure 3.5 Aligned nanofibers can increase the conversion efficiency of Tau-EGFP fibroblasts. Reprogramming efficiency of Tau-EGP fibroblasts transduced with BAM and cultured on blank membranes, random nanofibers, and aligned nanofibers (n=4) (*p<0.05).
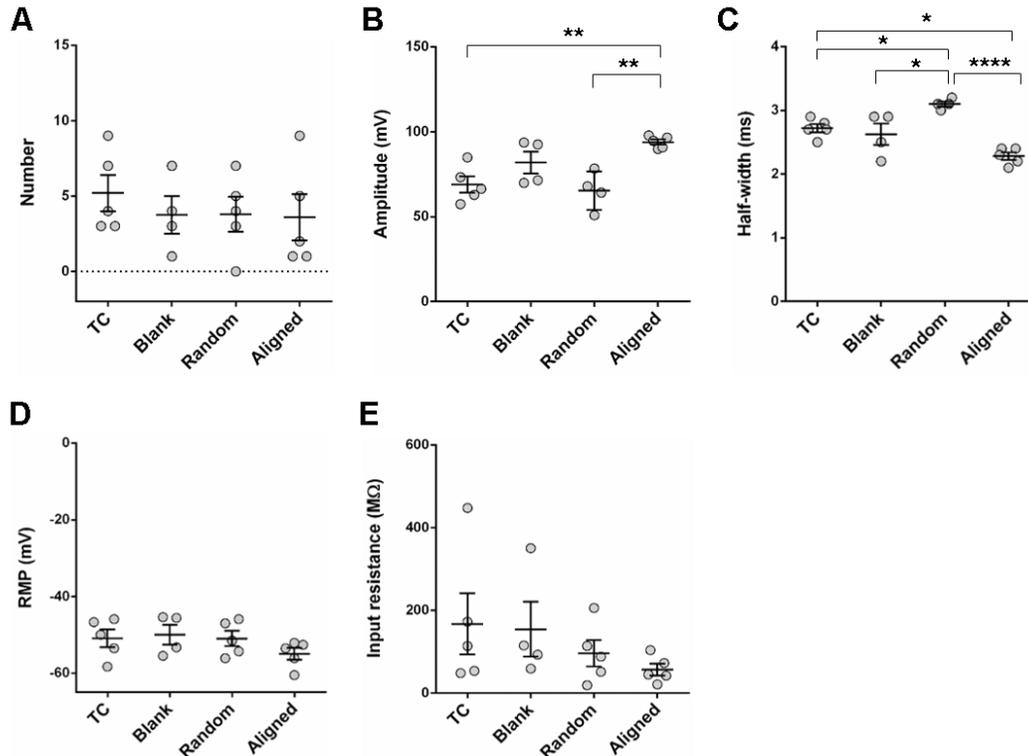
Figure 3.6 Electrophysiological analysis to assess the functionality of nanotopography-derived iN cells. A-E. Quantification of electrophysiological properties of iN cells generated on blank PC membranes, random and aligned nanofibers, and TCPS. Each circle represents an individual cell that was tested. The following were measured: number of action potentials (A), action potential amplitude (B) and half-width (C), resting membrane potential, RMP (D) and input resistance (E). Graphs show the mean $\pm$ one standard error of the mean (*$p<0.05$, **$p<0.01$, ****$p<0.0001$).

3.3.4 Aligned Nanofibers Can Promote Ascl1 Reprogramming

To gain insights into the mechanism by which nanotopography may regulate iN reprogramming efficiency, we then analyzed how nanofiber orientation can modulate neuronal gene expression. Fibroblasts were transduced with BAM and cultured on the nanofibers, TCPS, and blank PC membranes for 4 days followed by qRT-PCR analysis of various neuronal genes, including the key reprogramming factors. We found that neuronal gene expression was higher on aligned nanofibers compared to the other surfaces (Figure 3.7A). Of interest, aligned nanofibers upregulated the expression of Ascl1 to a greater extent than the other two reprogramming factors, Brn2 and Myt1l. It has been reported that Ascl1 plays a critical role in induced neuronal reprogramming as it has been identified as a pioneer factor and moreover, can generate iN cells when transduced alone[48,49]. As aligned nanofibers increased the expression of Ascl1, we further examined whether nanotopography could influence the conversion of fibroblasts into neurons with a single factor. Surprisingly, we observed that aligned nanofibers generated significantly more iN cells from fibroblasts transduced with only Ascl1 than random fibers (Figure 3.7B). The potential mechanisms that allow aligned nanofibrous membranes to modulate neuronal gene expression and Ascl1-mediated reprogramming are further being investigated.
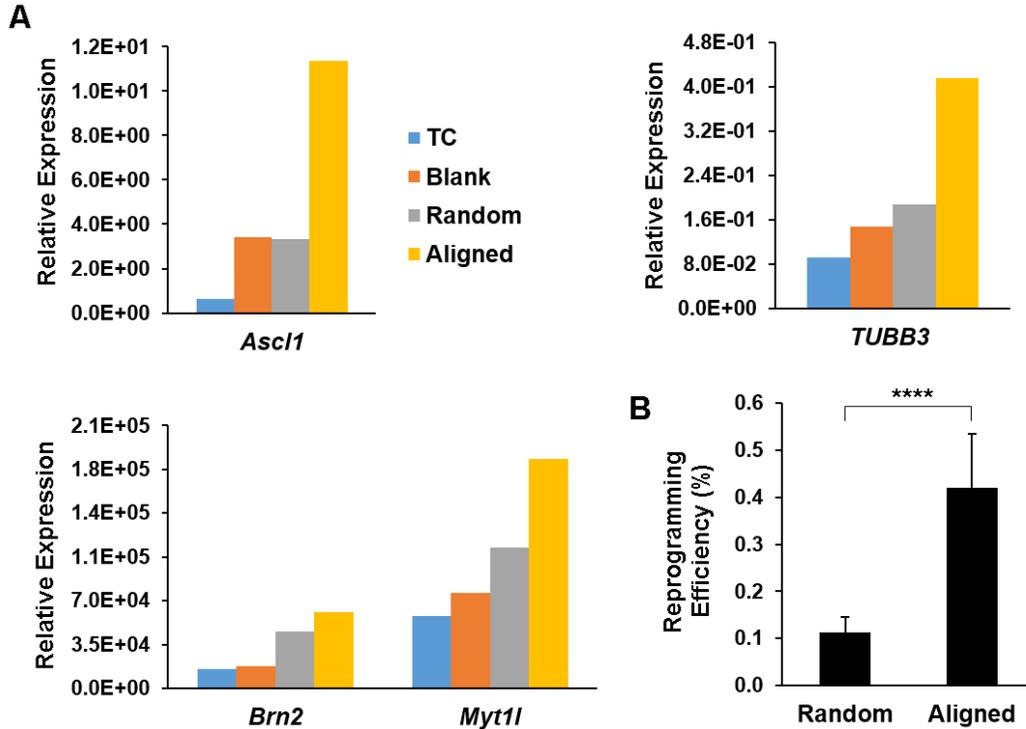
Figure 3.7 Nanotopography can modulate neuronal gene expression and promote Ascl1 reprogramming. A. qRT-PCR analysis of neuronal gene expression in BAM-transduced fibroblasts cultured on TCPS, blank membranes, random nanofibers and aligned nanofibers for 4 days (n=1). **B.** Reprogramming efficiency of Tau-EGFP fibroblasts transduced with Ascl1 and cultured on random and aligned nanofibers for 21 days (n=6) (*p<0.05).

In essence, findings from this study highlight the effects of micro- and nanotopography on the direct conversion of fibroblasts into neurons. We demonstrate that nanoscale cues, in particular aligned nanofibers, play a more significant role in modulating the conversion efficiency in comparison to microgrooves, suggesting that topographical cues can be used to further optimize cell reprogramming. Moreover, the iN cells generated on the various bioengineered substrates display functional neuronal properties. These iN cells can potentially serve as a new source of neurons for cell replacement therapies to combat neurodegenerative disorders and for the development of neurological disease models for drug discovery.

Chapter 4: Conclusion

4.1 Dissertation Conclusions

Early studies involving somatic cell nuclear transfer established the notion that the reverse process of differentiation is conceivable in a process now referred to as cell reprogramming. To date, there are two cell reprogramming strategies that have been identified to manipulate cell fate: induced pluripotent stem cell (iPSC) reprogramming and direct conversion. iPSC reprogramming allows for somatic cells, typically adult fibroblasts, to be reprogrammed into induced pluripotent stem cells through the overexpression of four transcription factors. These iPSCs, which resemble embryonic stem cells, are expandable and can be further used to yield new cell types through directed differentiation. These iPSC-derived cells offer the advantage of being autologouly sourced, however, careful consideration and purification steps must be taken into account to avoid risks of teratoma formation. Moreover, the entire process of iPSC derivation, expansion and directed differentiation is lengthy and costly. An alternative to such an approach is direct conversion, a process by which somatic cells can be converted into new cell types without proceeding through a pluripotent state. It can similarly be used to generate patient-specific cells, however, the overall derivation process is shorter.

While these two reprogramming strategies are promising approaches for disease modeling and regenerative medicine, they are far from being optimized as low conversion efficiencies remains to be one of the biggest challenges. As biochemical methods have been employed to improve reprogramming efficiency, biomaterials are increasingly being integrated to determine their influence on the reprogramming process with the goal of further optimizing the system. Biomaterials enable the creation of an *in vitro* synthetic niche that resembles the *in vivo* microenvironment in order to study cell processes in a more physiologically relevant system. Although there are several studies that highlight the role of biochemical and biophysical factors in iPSC reprogramming, their effects on direct reprogramming are not well understood.

Eukaryotic cells have cytoskeletons that span the cytoplasm to provide a structural link between the extracellular matrix and the nucleus. The cytoskeleton plays an important role in mechanotransduction as it enables the transmission of biophysical signals from the cell surface to the nucleus to affect the chromatin state. Although the cytoskeleton is involved in virtually all cellular processes, its role in direct reprogramming remains unknown.

Here, we show, for the first time, that disruption of the actin-myosin cytoskeleton using chemical compounds can significantly improve the direct reprogramming of adult fibroblasts into neurons. We found that blebbistatin, a non-muscle myosin II inhibitor, modulated the gene expression of fibroblasts to downregulate the mesenchymal phenotype and induce the neuronal phenotype. Further investigation showed that the mechanisms that govern blebbistatin-induced enhancement of induced neuronal reprogramming revolved around inhibition of focal adhesion signaling, brought upon by changes in the cell morphology. Interestingly, we observed that blebbistatin disrupted lamin A/C to influence induced neuronal conversion, demonstrating a novel role for nuclear membrane proteins in direct reprogramming. Lastly, we found that single factor reprogramming (i.e. Ascl1 alone) can be improved using blebbistatin.

In any given physiological microenvironment, cells may experience a number of biochemical and biophysical inputs that can alter cell behavior. Biophysical factors, such as topographical and mechanical properties of cell-adhesive substrates, have been shown to regulate a variety of cellular processes. However, the role of biophysical factors in direct reprogramming

is not fully understood. Therefore, we set out to investigate the effects of directly reprogramming fibroblasts into neurons on various topographical cues in conjunction with lentiviral delivery of neurogenic transcriptions factors, *Ascl1*, *Brn2*, and *Myt1l*. Topographical substrates consisted of poly(dimethylsiloxane) (PDMS) microgrooves and electrospun nanofibrous membranes with either a random or aligned fiber orientation and their effects were compared to traditional tissue culture polystyrene (TCPS). We found that we were able to generate induced neuronal (iN) cells on the various topographical surfaces and these cells displayed a typical neuronal morphology and expressed neuronal β-III tubulin (TUJ1). Microgrooves only slightly enhanced the reprogramming efficiency in comparison to flat PDMS membranes but yielded significantly more iN cells compared to TCPS. As PDMS membranes were able to significantly increase the reprogramming efficiency compared to TCPS, this suggests that a different material property (e.g. hydrophobicity) of PDMS membranes may influence induced neuronal reprogramming. Further examination on the effect of nanoscale cues demonstrated that nanofiber alignment significantly improved induced neuronal conversion. Characterization studies revealed that the derived iN cells exhibited mature, functional neuronal properties. Finally, we observed that aligned nanofibers were to modulate neuronal gene expression and further promoted the direct reprogramming of fibroblasts into neurons using Ascl1 alone. Our findings are in agreement with recent studies that have reported that microgratings and nanogrooved substrates can promote induced neuronal conversion[34,35].

Altogether, findings from our studies illustrate that biochemical and biophysical cues can regulate the direct reprogramming of fibroblasts into neurons. We demonstrate how small molecules and topographical cues can be used to further optimize direct reprogramming strategies and provide insights into the mechanisms that determine cell fate. These findings have important implications for the development of neurological disease models for drug discovery, in the design of next-generation biomaterials, and the field of regenerative medicine.

4.2 Future Directions

This work demonstrates that biochemical and biophysical cues can influence the direct reprogramming process, which is promising approach for disease modeling and personalized medicine. While our studies involving the use of mouse fibroblasts serve as a proof of concept and currently, most direct reprogramming strategies involving biomaterials have been performed *in vitro* using mouse models, in the future it will be interesting to see if the same phenomenon is observed when using human cells for direct reprogramming and whether the combination of biomaterials along with biochemical methods can be used to facilitate the *in vivo* application of such strategies. This will be important as it can demonstrate the clinical relevance of our findings and prove to be valuable for regenerative medicine.

As we determined that cytoskeletal disruption using small molecules can modulate induced neuronal conversion, it will also be practical to explore the involvement of the actomyosin cytoskeleton and nuclear lamina in the context of biophysical factors as this may help to further elucidate the mechanism by which topography can regulate direct reprogramming. Recent work from our lab has demonstrated that topographical cues can affect the cell epigenetic state to influence iPSC reprogramming[62]. Thus, future studies include to examine whether blebbistatin can modulate the chromatin state and/or epigenetic modifications to regulate direct conversion and whether nanotopography-induced epigenetic changes play any role in direct reprogramming.

Importantly, the underlying mechanisms by which biophysical factors can modulate signaling pathways to regulate direct reprogramming still await further investigation. Our findings show that blebbistatin and aligned nanofibers can modulate gene expression to influence induced neuronal conversion. However, it remains to be addressed whether these biochemical and biophysical cues are directly affecting gene expression and/or if there are any upstream signaling events that are leading to downstream changes in the gene expression pattern. Additionally, it is possible to examine the role of signaling molecules that are known to alter protein translocation to modulate gene activation and similarly, those involved in mechanotransductive pathways. For example, Sia *et al.* recently identified that the transcription factor Mkl1 functioned as a mechanotransducer that was activated on microgrooves and played a role in the topography-enhanced reprogramming of mouse fibroblasts into cardiomyocytes[36].

Moreover, as it has been shown that small molecules that inhibit SMAD and GSK3β signaling can significantly enhance the conversion of human fibroblasts into neurons[71], it will be interesting to determine whether nanotopography can modulate these signaling pathways to influence induced neuronal conversion in our system. By investigating cell signaling pathways and performing robust characterization of temporal gene expression during the reprogramming course, we can gain insights into the mechanisms that determine cell fate as well as potentially identify key molecular targets that can be used to further enhance the cell reprogramming process. Furthermore, these findings can also be used to direct the engineering of biomaterials that can mimic the induction of such gene expressions in order to improve conversion efficiencies.

In closing, our findings aid to broaden our understanding of the role of biophysical factors in cell reprogramming and the mechanotransductive mechanisms that may be involved. The outcomes from the proposed future studies can have important consequences for personalized medicine as the generation of patient-specific cells provides an exciting opportunity to expand our knowledge of disease pathophysiology that can lead to the development of new therapeutics.

References

1. Gurdon, JB. Uehlinger, V. © 1958 Nature Publishing Group. (1958).
2. Takahashi, K. & Yamanaka, S. Induction of pluripotent stem cells from mouse embryonic and adult fibroblast cultures by defined factors. *Cell* **126,** 663–76 (2006).
3. Davis, R. L., Weintraub, H. & Lassar, a B. Expression of a single transfected cDNA converts fibroblasts to myoblasts. *Cell* **51,** 987–1000 (1987).
4. Vierbuchen, T. *et al.* Direct conversion of fibroblasts to functional neurons by defined factors. *Nature* **463,** 1035–41 (2010).
5. Pang, Z. P. *et al.* Induction of human neuronal cells by defined transcription factors. *Nature* **476,** 220–3 (2011).
6. Ieda, M. *et al.* Direct reprogramming of fibroblasts into functional cardiomyocytes by defined factors. *Cell* **142,** 375–86 (2010).
7. Szabo, E. *et al.* Direct conversion of human fibroblasts to multilineage blood progenitors. *Nature* **468,** 521–6 (2010).
8. Sekiya, S. & Suzuki, A. Direct conversion of mouse fibroblasts to hepatocyte-like cells by defined factors. *Nature* **475,** 390–3 (2011).
9. Huang, P. *et al.* Direct reprogramming of human fibroblasts to functional and expandable hepatocytes. *Cell Stem Cell* **14,** 370–84 (2014).
10. Zhou, H. *et al.* Generation of Induced Pluripotent Stem Cells Using Recombinant Proteins. *Cell Stem Cell* **4,** 581 (2009).
11. Yu, J. *et al.* Human Induced Pluripotent Stem Cell Free of Vector Transgene Sequences. *Science (80-.).* **324,** 797–801 (2009).
12. Warren, L. *et al.* Highly Efficient Reprogramming to Pluripotency and Directed Differentiation of Human Cells with Synthetic Modified mRNA. *Cell Stem Cell* **7,** 618–630 (2010).
13. Anokye-Danso, F. *et al.* Highly efficient miRNA-mediated reprogramming of mouse and human somatic cells to pluripotency. *Cell Stem Cell* **8,** 376–88 (2011).
14. Miyoshi, N. *et al.* Reprogramming of mouse and human cells to pluripotency using mature microRNAs. *Cell Stem Cell* **8,** 633–638 (2011).
15. Hou, P. *et al.* Pluripotent Stem Cells Induced from Mouse Somatic Cells by Small-Molecule Compounds. *Science (80-.).* **341,** 651–654 (2013).
16. Li, X. *et al.* Small-Molecule-Driven Direct Reprogramming of Mouse Fibroblasts into Functional Neurons. *Cell Stem Cell* **17,** 195–203 (2015).
17. Hu, W. *et al.* Direct Conversion of Normal and Alzheimer's Disease Human Fibroblasts into Neuronal Cells by Small Molecules Cell Stem Cell Direct Conversion of Normal and Alzheimer's Disease Human Fibroblasts into Neuronal Cells by Small Molecules. *Stem Cell* **17,** 204–212 (2015).
18. Cao, N. *et al.* Conversion of human fibroblasts into functional cardiomyocytes by small molecules. *Science* aaf1502 (2016). doi:10.1126/science.aaf1502
19. Human, S. *et al.* Nanotopography In fl uences Adhesion , Embryonic Stem Cells. 4094–4103 (2012).
20. Kim, D.-H. *et al.* Mechanosensitivity of fibroblast cell shape and movement to anisotropic substratum topography gradients. *Biomaterials* **30,** 5433–44 (2009).
21. Dulgar-Tulloch, a J., Bizios, R. & Siegel, R. W. Human mesenchymal stem cell adhesion and proliferation in response to ceramic chemistry and nanoscale topography. *J. Biomed.*

Mater. Res. A **90,** 586–94 (2009).

22.   Pelham, R. J. & Wang, Y. L. Cell locomotion and focal adhesions are regulated by the mechanical properties of the substrate. *Biol. Bull.* **194,** 348–350 (1998).

23.   Patel, S. *et al.* Bioactive nanofibers: synergistic effects of nanotopography and chemical signaling on cell guidance. *Nano Lett.* **7,** 2122–8 (2007).

24.   Engler, A. J., Sen, S., Sweeney, H. L. & Discher, D. E. Matrix elasticity directs stem cell lineage specification. *Cell* **126,** 677–89 (2006).

25.   McBeath, R., Pirone, D. M., Nelson, C. M., Bhadriraju, K. & Chen, C. S. Cell shape, cytoskeletal tension, and RhoA regulate stem cell lineage commitment. *Dev. Cell* **6,** 483–95 (2004).

26.   Chowdhury, F. *et al.* Material properties of the cell dictate stress-induced spreading and differentiation in embryonic stem cells. *Nat. Mater.* **9,** 82–8 (2010).

27.   Park, J. S. *et al.* The effect of matrix stiffness on the differentiation of mesenchymal stem cells in response to TGF-β. *Biomaterials* **32,** 3921–30 (2011).

28.   Lam, H. J., Patel, S., Wang, A., Chu, J. & Li, S. In Vitro Regulation of Neural Differentiation and Axon Growth by Growth Factors and Bioactive Nanofibers. *Tissue Eng. Part A* **16,** 2641–2648 (2010).

29.   Saha, K. *et al.* Substrate modulus directs neural stem cell behavior. *Biophys. J.* **95,** 4426–38 (2008).

30.   Yoo, A. S. *et al.* MicroRNA-mediated conversion of human fibroblasts to neurons. *Nature* **476,** 228–31 (2011).

31.   Ambasudhan, R. *et al.* Direct reprogramming of adult human fibroblasts to functional neurons under defined conditions. *Cell Stem Cell* **9,** 113–8 (2011).

32.   Jayawardena TM, Egemnazarov B, F. E. et al. MicroRNA- mediated in vitro and in vivo direct reprogramming of cardiac fibroblasts to cardiomyocytes. *Circ Res* **110,** 1465–1473 (2013).

33.   Xue, Y. *et al.* Direct conversion of fibroblasts to neurons by reprogramming PTB-regulated microRNA circuits. *Cell* **152,** 82–96 (2013).

34.   Kulangara, K. *et al.* The effect of substrate topography on direct reprogramming of fibroblasts to induced neurons. *Biomaterials* 1–10 (2014). doi:10.1016/j.biomaterials.2014.03.034

35.   Yoo, J. *et al.* Nanogrooved substrate promotes direct lineage reprogramming offibroblasts to functional induced dopaminergic neurons. *Biomaterials* **45,** 36–45 (2015).

36.   Sia, J., Yu, P., Srivastava, D. & Li, S. Effect of biophysical cues on reprogramming to cardiomyocytes. *Biomaterials* **103,** 1–11 (2016).

37.   Fletcher, D. A. & Mullins, R. D. Cell mechanics and the cytoskeleton. *Nature* **463,** 485–492 (2010).

38.   Limouze, J., Straight, A. F., Mitchison, T. & Sellers, J. R. Specificity of blebbistatin, an inhibitor of myosin II. *J. Muscle Res. Cell Motil.* **25,** 337–341 (2004).

39.   Kov??cs, M., T??th, J., Het??nyi, C., M??ln??si-Csizmadia, A. & Seller, J. R. Mechanism of blebbistatin inhibition of myosin II. *J. Biol. Chem.* **279,** 35557–35563 (2004).

40.   Watanabe, M. *et al.* Blebbistatin, a myosin II inhibitor, suppresses contraction and disrupts contractile filaments organization of skinned taenia cecum from guinea pig. *Am. J. Physiol. Cell Physiol.* **298,** C1118–C1126 (2010).

41.   Ishizaki, T. *et al.* Pharmacological properties of Y-27632, a specific inhibitor of rho-associated kinases. *Mol. Pharmacol.* **57,** 976–983 (2000).

42. Samson, F., Donoso, J. a, Heller-Bettinger, I., Watson, D. & Himes, R. H. Nocodazole action on tubulin assembly, axonal ultrastructure and fast axoplasmic transport. *J. Pharmacol. Exp. Ther.* **208,** 411–417 (1979).

43. Van De Willige, D., Hoogenraad, C. C. & Akhmanova, A. Microtubule plus-end tracking proteins in neuronal development. *Cell. Mol. Life Sci.* **73,** 2053–2077 (2016).

44. Danowski, B. A. Fibroblast contractility and actin organization are stimulated by microtubule inhibitors. *J. Cell Sci.* **93,** 255–266 (1989).

45. Alenghat, F. J. & Ingber, D. E. Mechanotransduction: all signals point to cytoskeleton, matrix, and integrins. *Sci. STKE* **2002,** pe6 (2002).

46. Wang, N., Tytell, J. D. & Ingber, D. E. Mechanotransduction at a distance: mechanically coupling the extracellular matrix with the nucleus. *Nat. Rev. Mol. Cell Biol.* **10,** 75–82 (2009).

47. Tajik, A. *et al.* Transcription upregulation via force-induced direct stretching of chromatin. *Nat. Mater.* **1,** (2016).

48. Wapinski, O. L. *et al.* Hierarchical mechanisms for direct reprogramming of fibroblasts to neurons. *Cell* **155,** 621–35 (2013).

49. Chanda, S. *et al.* Generation of induced neuronal cells by the single reprogramming factor ASCL1. *Stem Cell Reports* **3,** 282–296 (2014).

50. Brown, R. C., Lockwood, A. H. & Sonawane, B. R. Neurodegenerative diseases: An overview of environmental risk factors. *Environ. Health Perspect.* **113,** 1250–1256 (2005).

51. Ramanan, V. K. & Saykin, A. J. Pathways to neurodegeneration: mechanistic insights from GWAS in Alzheimer's disease, Parkinson's disease, and related disorders. *Am. J. Neurodegener. Dis.* **2,** 145–75 (2013).

52. Son, E. Y. *et al.* Conversion of mouse and human fibroblasts into functional spinal motor neurons. *Cell Stem Cell* **9,** 205–18 (2011).

53. Qiang, L. *et al.* Directed conversion of Alzheimer's disease patient skin fibroblasts into functional neurons. *Cell* **146,** 359–71 (2011).

54. Pfisterer, U. *et al.* Direct conversion of human fibroblasts to dopaminergic neurons. *Proc. Natl. Acad. Sci. U. S. A.* **108,** 10343–8 (2011).

55. Caiazzo, M. *et al.* Direct generation of functional dopaminergic neurons from mouse and human fibroblasts. *Nature* **476,** 224–7 (2011).

56. Pang, Z. P. *et al.* Induction of human neuronal cells by defined transcription factors. *Nature* **476,** 220–3 (2011).

57. Ferrari, A. *et al.* Nanotopographic control of neuronal polarity. *Nano Lett.* **11,** 505–11 (2011).

58. Mahairaki, V. *et al.* Nanofiber Matrices Promote the Neuronal Differentiation of Human Embryonic Stem Cell-Derived Neural Precursors In Vitro. **17,** (2011).

59. Shahbazi, E. & Kiani, S. Electrospun nanofibrillar surfaces promote neuronal differentiation and function from human embryonic stem cells. *... Eng. Part A* **17,** (2011).

60. Ren, Y.-J. *et al.* Enhanced differentiation of human neural crest stem cells towards the Schwann cell lineage by aligned electrospun fiber matrix. *Acta Biomater.* **9,** 7727–36 (2013).

61. Qi, L. *et al.* The effects of topographical patterns and sizes on neural stem cell behavior. *PLoS One* **8,** e59022 (2013).

62. Downing, T. L. *et al.* Biophysical regulation of epigenetic state and cell reprogramming.

Nat. Mater. **12,** 1154–62 (2013).

63. Zhu, Y. *et al.* Engineering bi-layer nanofibrous conduits for peripheral nerve regeneration. *Tissue Eng. Part C. Methods* **17,** 705–15 (2011).

64. Li, Y. *et al.* Biophysical regulation of histone acetylation in mesenchymal stem cells. *Biophys. J.* **100,** 1902–9 (2011).

65. Baron-Van Evercooren, A. *et al.* Nerve growth factor, laminin, and fibronectin promote neurite growth in human fetal sensory ganglia cultures. *J. Neurosci. Res.* **8,** 179–193 (1982).

66. Powell, S. K., Williams, C. C., Nomizu, M., Yamada, Y. & Kleinman, H. K. Laminin-like proteins are differentially regulated during cerebellar development and stimulate granule cell neurite outgrowth in vitro. *J. Neurosci. Res.* **54,** 233–247 (1998).

67. Barros, C. S., Franco, S. J. & Müller, U. Extracellular matrix: functions in the nervous system. *Cold Spring Harb Perspect Biol.* **3,** a005108 (2011).

68. Lim, S. H., Liu, X. Y., Song, H., Yarema, K. J. & Mao, H.-Q. The effect of nanofiber-guided cell alignment on the preferential differentiation of neural stem cells. *Biomaterials* **31,** 9031–9 (2010).

69. Wang, J. *et al.* The effects of electrospun TSF nanofiber diameter and alignment on neuronal differentiation of human embryonic stem cells. *J. Biomed. Mater. Res. A* **100,** 632–45 (2012).

70. Jiang, X. *et al.* Nanofiber topography and sustained biochemical signaling enhance human mesenchymal stem cell neural commitment. *Acta Biomater.* **8,** 1290–302 (2012).

71. Ladewig, J. *et al.* Small molecules enable highly efficient neuronal conversion of human fibroblasts. *Nat. Methods* **9,** 575–8 (2012).